minerals

MDPI

Article

U–Pb Zircon Geochronological and Petrologic Constraints on the Post-Collisional Variscan Volcanism of the Tiddas-Souk Es-Sebt des Aït Ikko Basin (Western Meseta, Morocco)

Ismail Hadimi [1,*], Nasrrddine Youbi [1,2], Abdelhak Ait Lahna [1], Mohamed Khalil Bensalah [1,3], Oussama Moutbir [1], João Mata [3], Miguel Doblas [4], Colombo Celso Gaeta Tassinari [5], Laura Gaggero [6], Miguel Angelo Stipp Basei [7], Kei Sato [5], Warda El Moume [1] and Moulay Ahmed Boumehdi [1,3]

1 Department of Geology, Faculty of Sciences-Semlalia, Cadi Ayyad University, Prince Moulay Abdellah Boulevard, Marrakech P.O. Box 2390, Morocco; youbi@uca.ac.ma (N.Y.); aitlahna.abdelhak@gmail.com (A.A.L.); bensalah@uca.ac.ma (M.K.B.); oussama.moutbir2@gmail.com (O.M.); warda.elmoume@gmail.com (W.E.M.); boumehdi@uca.ac.ma (M.A.B.)
2 Faculty of Geology and Geography, Tomsk State University, 634050 Tomsk, Russia
3 Instituto DomLuiz, Faculdade de Ciências, Universidade de Lisbona, 1749-016 Lisboa, Portugal; jmata@fc.ul.pt
4 Instituto de Geociencias (CSIC-UCM), Ciudad Universitaria, c/Doctor Severo Ochoa 7, 28040 Madrid, Spain; m.doblas@igeo.ucm-csic.es
5 Centro de Pesquisas Geocronológicas (CPGeo), Instituto de Geociências (IG), Universidade de São Paulo—USP, São Paulo 05422-970, Brazil; ccgtassi@usp.br (C.C.G.T.); keisato@usp.br (K.S.)
6 Department of Earth, Environment and Life Sciences, University of Genoa, Corso Europa 26, 16132 Genoa, Italy; laura.gaggero@unige.it
7 Instituto de Geociências (IG), Departamento de Mineralogia e Geotectônica (GMG), Universidade de São Paulo—USP, Rua do Lago, 562 Cidade Universitária, São Paulo 05508-080, Brazil; baseimas@usp.br
* Correspondence: ismail.hadimi@gmail.com

Abstract: The NE–SW trending Tiddas Souk Es-Sebt des Ait Ikko (TSESDAI) basin, located at 110 km southeast of Rabat, in the region of Khmesset between the village of Tiddas and Souk Es-Sebt des Ait Ikko, is the third largest late Palaeozoic continental trough in the northern Central Moroccan Meseta. It is a ~20 km long and ~2–3 km wide basin, comprising mainly mixed volcano-sedimentary reddish-purple continental Permian rocks laying with an angular unconformity on Visean deep marine siliciclastic sediments and unconformably overlain by the Triassic and Cenozoic formations. In this study we aim to better determine the age of Permian volcanics and their chemical and mineralogical characteristics, as well as assess the provenance of inherited zircons, thus contributing to the understanding of the late stages of the Variscan orogeny in Morocco. The standard volcanic succession includes the following terms: (i) andesites, lapilli tuffs and andesitic ash deposits; (ii) accumulations of rhyolitic lavas; (iii) lapilli tuffs and rhyolitic ash (formation F1); (iv) flows and breccias of dacites; (v) andesite flows; and (vi) basaltic flows. The various volcanic and subvolcanic studied rocks display calc-alkaline-series characteristics with high contents of SiO_2, Al_2O_3, CaO, MgO, and relatively abundant alkalis, and low contents of MnO. In the classification diagram, the studied facies occupy the fields of andesites, trachy-basalts, dacites, trachydacites, and rhyolites and display a sub-alkaline behavior. These lavas would be derived from a parental mafic magma (basalts) produced by partial fusion of the upper mantle. Specific chemical analyses that were carried out on the mineralogical phases (biotite and pyroxene) revealed that the examined biotites can be classified as magnesian and share similarities with the calc-alkaline association-field, while the clinopyroxenes are mainly augites and plot on the calc-alkaline orogenic basalt field. Andesites and dacites of TSESDAI show similarities with the rocks of the calc-alkaline series not linked to active subduction and which involve a continental crust in their genesis. The existence of enclaves in the lavas of the TSESDAI massif; the abnormally high contents of Rb, Ba, Th, and La; and the systematic anomalies in TiO_2 and P_2O_5 indicate also a crustal contamination mechanism. Three magmatic episodes are distinguished with two episodes that correspond to an eruptive cycle of calc-alkaline andesites and rhyolites followed

check for updates

Citation: Hadimi, I.; Youbi, N.; Ait Lahna, A.; Bensalah, M.K.; Moutbir, O.; Mata, J.; Doblas, M.; Tassinari, C.C.G.; Gaggero, L.; Basei, M.A.S.; et al. U–Pb Zircon Geochronological and Petrologic Constraints on the Post-Collisional Variscan Volcanism of the Tiddas-Souk Es-Sebt des Aït Ikko Basin (Western Meseta, Morocco). *Minerals* **2021**, *11*, 1099. https://doi.org/10.3390/min11101099

Academic Editors: Wilfried Winkler and Albrecht von Quadt

Received: 29 August 2021
Accepted: 30 September 2021
Published: 7 October 2021

Publisher's Note: MDPI stays neutral with regard to jurisdictional claims in published maps and institutional affiliations.

by a basaltic episode. The SHRIMP U–Pb geochronologic data of zircons recovered from the rhyolite dome of Ari El Mahsar in TSESDAI basin show a Concordia age of 286.4 ± 4.7 Ma interpreted to date the magmatic crystallization of this dome. Thus, the rhyolite likely belongs to the third magmatic episodes of TSESDAI.

Keywords: Western Hercynian Meseta; Permian basin; Tiddas Souk Es-Sebt des ait ikko volcanic basin; U–Pb geochronology; mineralogy; petrology

1. Introduction

The European Northwest African Magmatic Province (EUNWA or EUNWAMP; e.g., [1–3] was emplaced during Late Carboniferous–Permian times and has been linked to the gravitational collapse of the previously overthickened and weakened Variscan orogenic belt. The gravitational collapse of the Variscan edifice occurred through simple pure shear low-angle extensional detachments during the late Carboniferous–Permian, giving rise to a Basin and Range type extensional province in Europe, and northwestern Africa involving the unroofing of large metamorphic core complexes and synextensional plutonic bodies, dike and sill swarms, and volcanic successions. Coevally with this extensional scenario, Europe and northwestern Africa were affected by a complex system of conjugate strike-slips faults (NE–SW sinistral and NW–SE dextral), which partially disrupted the Variscan edifice, resulting in new Permo-Carboniferous stress patterns with the principal compressional axis oriented N–S [4,5]. This episode was accompanied by sediment deposition and volcanism in transtensional and pull-apart basins [1,6,7]. This episode resulted from a major dextral transcurrent movement along an intracontinental shear zone located between Gondwana and Laurussia [4,5,8,9]. To date, a range of chronometers has been applied to determine crystallization ages from across the region of the EUNWA Large Igneous Province, including whole-rock Rb–Sr and K–Ar dating; $^{40}Ar/^{39}Ar$ dating of mineral separates; and U–Pb dating of zircon, titanite, and perovskite (e.g., [10]). The duration of activity is currently estimated to span a period of ca. 100 million years, from the Early Carboniferous to the Late Permian–Early Triassic (350–250 Ma), with several hiatuses [11]. Three main pulses can be distinguished at ca. 300 Ma, 290–275 Ma, and 250 Ma, and each of these pulses can be considered a separate LIP within the overall EUNWA Large Igneous Province. These eruptive cycles are well represented in Morocco in northwestern Africa and also in southern Scandinavia and northern Germany. The huge volume of extruded and intruded magmatic products of the EUNWA province (in the Oslo Graben, the estimated volume is 35,000 km^3, while in the North German Basin, the total volume of felsic volcanic rocks, mainly rhyolites and rhyodacites, was of the order of 48,000 km^3) has led to suggestions of a thermally anomalous mantle plume to explain this magmatic pulse [12,13]. A significant problem of the plume hypothesis is the duration of activity and the helium isotope signature of lithospheric mantle xenoliths from the Scottish Permo-Carboniferous dikes, sills, and vents [14]. The EUNWA magmatic province may have contributed to the great Gondwanan glaciation that occurred from the late Devonian to the late Permian [15–17]. Glaciers achieved their maximum paleolatitudinal range between the middle Stephanian (ca. 305 Ma ago) and the end of the Sakmarian (ca. 284 Ma ago) [17]. This hypothesis is termed the icehouse-silicic large igneous province (SLIP) hypothesis [18].

In Morocco, the Permian sedimentation was continental and occurred in small isolated basins (Khenifra, Boudoufoud, Bou-Achouch, Tiddas Souk Es-Sebt des Aït Ikko (TSESDAI), Chougrane, Mechraa Ben Abbou, Senhaja, Ouelad Maachou, Ourika, and Argana; see Figure 1), mostly originated as NE–SW to NNE–SSW half-graben-like structures, during the gravitational collapse of the Variscan orogenic belt [19–22]. They are the remnants of strongly subsided intramountainous troughs predominantly filled with red-colored detritus, often associated with andesitic and rhyolitic lava flows, domes, pyroclastic rocks, and shallow-level dikes and sills. These volcanic basins and their associated plumbing

systems belong to the European Northwest African Magmatic Province (EUNWAMP); e.g., [1]).

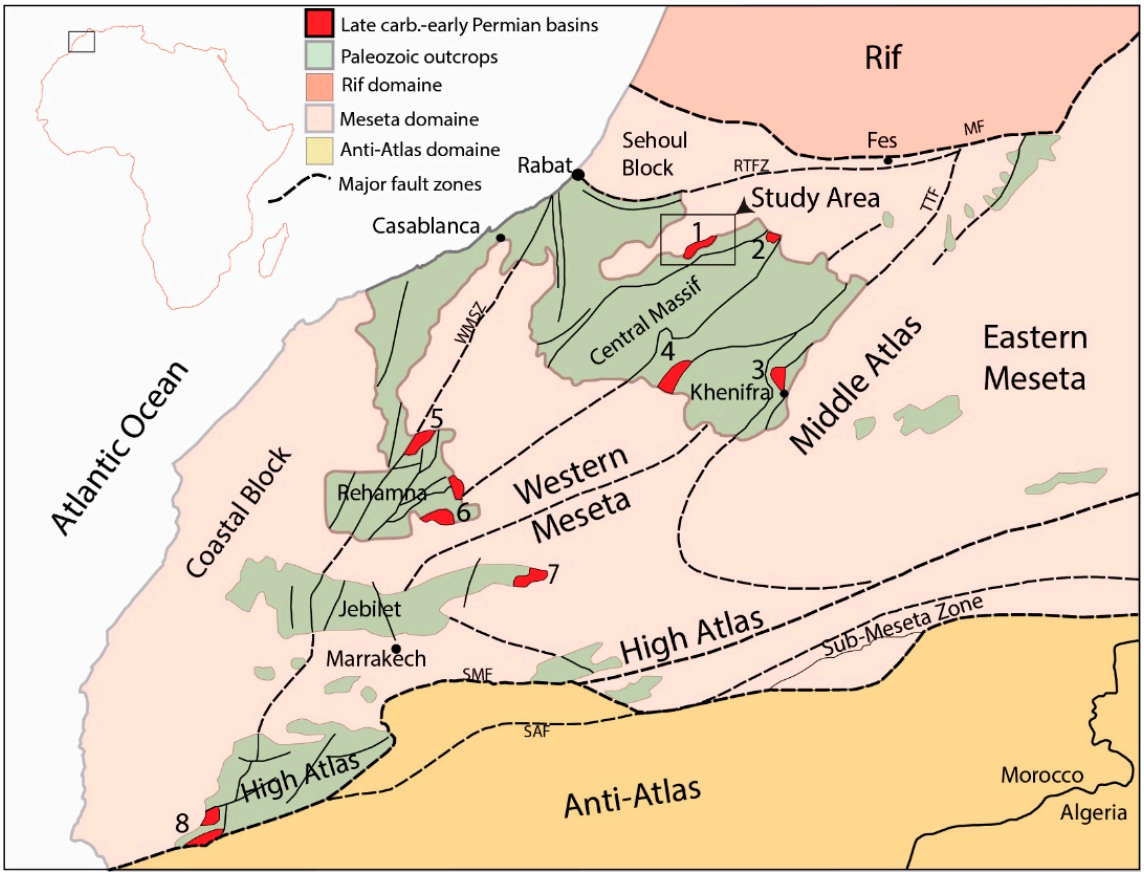

Figure 1. Principal tectonic domains of central Morocco (modified after [23–26]). Numbers 1–8 correspond to Carboniferous–Early Permian basins (1: the studied outcrops of Tiddas; 2: Bou Achouch, 3: Khenifra, 4: Chougrane, 5: Mechra ben Abbou, 6: Nzalet el Hararcha, 7: Senhaja, 8: Souss). Abbreviations: MF, Maghrebide Front; RTFZ, Rabat Tiflet Fault Zone; SAF, South Atlas Fault; SMF, South Meseta Fault; TTF, Tizi n' Tretten Fault Zone; WMSZ, Western Meseta Shear Zone.

While several Late Carboniferous–Permian basins have been extensively studied for their stratigraphic, paleontological, and sedimentological characteristics, very little is known on the petrology, geochemistry, and geochronology, with the exception of the recent work of [23]. In this study, we focus on TSESDAI Permian volcanism affecting the northwestern Gondwanaland margin in order to (1) determine, using a sensitive high-resolution ion microprobe (SHRIMP) the zircon U–Pb age of volcanic crystallization; (2) assess the provenance of inherited zircons; (3) describe the mineral chemistry of the main rock-forming minerals; (4) characterize geochemically the magma affinities; and (5) discuss the petrogenesis of volcanic rocks.

2. Geological Background

The NE–SW TSESDAI basin is located 110 km to the SE of Rabat (Figure 1), in the region of Khemisset (between the villages of Tiddas and Souk Es Sebt des Ait Ikko) and is the third-largest late Palaeozoic continental trough in the northern Central Moroccan Meseta. It is a ~20 km long and ~2–3 km wide basin, comprising mainly mixed volcanic–sedimentary reddish-purple Permian rocks laying with an angular unconformity on Visean deep marine siliciclastic sediments and being unconformably overlain by the Triassic and Cenozoic formations (Figure 2). The volcanic/subvolcanic formations of this basin consist of rhyolitic domes with associated rhyolitic dike swarms and andesitic to dacitic flows with a relatively reduced extension. These magmatic formations occupy an area

of about 48 km^2 and display massive textures and tabular surfaces. They are aligned along a NE–SW direction corresponding to the orientation of the major Hercynian to late Hercynian structures. These volcanics are intruded by a dike swarm with a NE–SW dominant direction and covered by Triassic and Tertiary deposits [19,27–29]. The red sedimentary package (40 to 300 m thick) of this basin is generally incomplete due to faulting. Three main formations have been recognized on the TSESDAI basin by [30–33]: (i) A 100 m-thick lower formation (F1) constituted by purple–red silty argillites, alternating with conglomerates including andesites, quartz, quartzite, sandstone, and rare limestones pebbles; (ii) an intermediate formation (F2) of about 120 m thick, consisting of silty argillites gullied and interspersed with channel deposits (e.g., puddingstones and coarse sandstone) with lenticular stratification and oblique tabular/horizontal bedding (the paleocurrents are directed towards the SW and S); and (iii) an upper formation (F3) of 50 to 80 m thick that is marked by thick red silty argillites interspersed with sandstone in centimetric to decametric benches. Determining the Permian age of these formations was constrained by using plant remains and vertebrate ichnofossils (e.g., [33,34]). The age has been recently confirmed by [35]. The occurrence of volcanics in this basin was first reported and termed by [36], being considered part, with those of the Khenifra Basin, of the so-called "Central Moroccan volcanic axis", extending from Khenifra to TSESDAI basins and displaying felsic and mafic volcanics overlain by Neogene/Quaternary formations. Until the 1980s, this "axial-model" has been accepted by several authors (e.g., [37] and references therein). Later on, many contributions largely improved the geological knowledge of this basin (e.g., [6,27,29]). The main conclusions of these authors are as follows: (i) The age of the TSESDAI basin volcanic complex is Permian s.l. (late-Carboniferous and pre-Triassic, probably Stephanian/Permian). (ii) There is a distinction of three major volcanic pulses, the first one (mainly andesitic) predating the Permian series. Witnesses of this pulse have been observed in the Tiddas region; however, most of this material is reworked within the conglomerates. The second pulse is synsedimentary and displays various interesting petrographic characteristics and remarkable andesitic lava flows interbedded within the detrital sediments. The third pulse consists of intrusive rhyolitic dikes that precede the Ari el Mahsar rhyolitic dome emplacement and the dacitic flows. (iii) There has been identification of three intra-Permian tectonic events. The close relationship between volcanism and fracturation is obvious; dikes and effusive centers are aligned along N40–N70, mostly strike-slip faults.

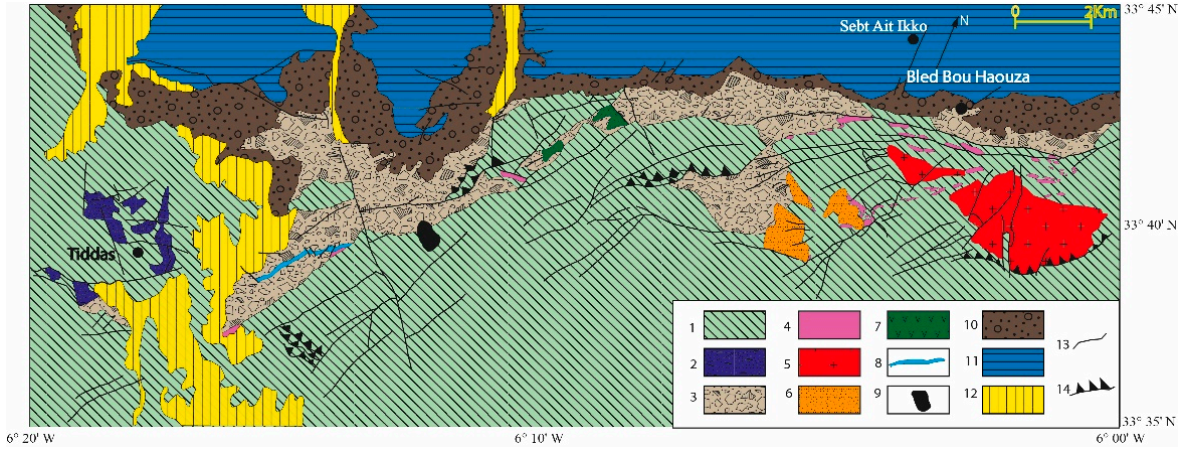

Figure 2. Geological map of the TSESDAI volcanic complex and its environs (based on [28], completed by [29,38]): 1. Upper Visean Paleozoic terrains (schists and quartzites); 2. pyroxene andesties (Tiddas andesites); 3. Permian conglomerates, sandstones, and argillites; 4. biotite rhyolite dikes; 5. biotite rhyolitic dome (Ari Almahsar and Agrued El khebiza); 6. pyroxene dacites (Bled Bou Haouza); 7. olivine and pyroxene andesites (Sebt Ait ikko); 8. pyroxene dolerite vein; 9. pyroxene basalt flows of El Gitoune; 10. Triassic detrital and volcanic formations; 11. Messinian and Pliocene conglomeratic and marl formations; 12. Quaternary; 13. undefined faults; 14. inverse faults.

The assignment of the TSESDAI basin to the Permian was based on (a) the intrusion of rhyolites into the Visean deep marine siliciclastics (e.g., shark-thin rhyolitic extrusive dome of Ari el Mahsar and its satellite dikes); (b) the angular unconformity between the Visean siliciclastics folded during the late Westphalian A and red detrital sediments; (c) the presence of reworked rhyolitic/andesitic pebbles in the red sediments of this basin and their absence in the detrital sediments of the Westphalian C/D preserved nearby in the Sidi Kacem graben; (d) the angular unconformity between the Triassic and the red detrital sediments; and (e) a strike-slip fault that postdates the basin sedimentary/volcanic formations and predates the Triassic/Cenozoic.

3. Sampling and Analytical Procedures

3.1. Sampling

In order to investigate the nature, the tectonic setting, and the petrogenetic processes of the post-collisional Variscan volcanism of the TSESDAI basin, we collected and analyzed a total of eighteen samples from the least weathered outcrops (major and trace elements; Table 1). Nine chemicals analyses of [19,28] were used for comparison. In addition, a sample from the shark-fin-like rhyolitic extrusive dome of Ari el Mahsar (sample ARM15; N 30°48′45.7″, W 7°32′29.1″) was dated using SHRIMP U–Pb zircon geochronology (Figure 14, Table 2). Specific chemical analyzes were carried out on the mineralogical phases (pyroxene; Tables S1 and S2, biotite; Table S3) to characterize them and to determine the physicochemical conditions of the crystallization of the studied rocks. The pyroxenes selected for this study were exclusively from dacites given their better preservation in comparison with those of the andesites, which are mostly transformed into secondary minerals (chlorite, calcite, and silica).

3.2. Analytical Procedures

3.2.1. U–Pb Geochronology: Sensitive High-Resolution Ion Microprobe (SHRIMP IIe)

Igneous zircon grains from the shark-fin-like rhyolitic extrusive dome of the Ari el Mahsar sample ARM15 was separated for U–Pb age determinations at the CPGeo-USP, Brazil. The crystals were further mounted, together with the TEMORA-2 standard [39], in epoxy and polished to expose the interior of the grains. After coating with Au, the polished mounts were comprehensively examined with a FEI Quanta 250 scanning electron microscope equipped with secondary electrons and cathodoluminescence (CL) detectors at CPGeo-USP; the most common conditions used in CL analysis were as follows: 60 μA emission current, 15.0 kV accelerating voltage, 7 μm beam diameter, 200 μs acquisition time, and a resolution of 1024 × 884. The same mounts were analyzed afterwards by the U–Pb isotopic technique using a SHRIMP II following the analytical procedures of [40]. Correction for common Pb was made based on the ^{204}Pb measured, and the typical error for the ^{206}Pb/^{238}U ratio was less than 2%; uranium abundance and U/Pb ratios were calibrated against the TEMORA standard, and the ages were calculated using the Isoplot® (version$^{3.0}$, Berkeley Geochronology Center, Berkeley, CA, USA) application of [41]. Errors were reported as 1σ deviations, and ages were calculated at the 95% confidence level.

Table 1. Chemical compositions in major and traces elements of Tiddas-Souk Es Sebt des Ait Ikko volcanic complex magmatic rocks added to nine whole rock chemical analyses available in the literature (identified by an asterisk (*); [19,28]). Mg # = (MgO/40.32)/(Fe2O3t*0.9/71.8) + (MgO/40.32).

No Fac.	**1**	**1**	**2**	**2**	**2**	**2**	**2**	**2**	**2**	**2**	**3**	**3**	**3**	**3**
No Samp.	**YK48**	**YK49**	**YK37**	**YK44**	**YK43**	**YK32**	**YK27**	**YK1**	**W184 ***	**W186 ***	**YK6**	**W183A ***	**W181 ***	**W183B ***
SiO_2	54.12	56.21	63.90	64.83	64.85	65.39	65.85	65.86	66.47	67.85	67.18	68.35	68.82	68.82
TiO_2	1.04	1.03	0.73	0.69	0.69	0.59	0.64	0.59	0.70	0.66	0.24	0.29	0.32	0.35
Al_2O_3	15.99	15.88	15.79	15.33	15.45	15.22	15.10	14.93	14.20	14.05	14.73	13.99	14.55	14.12
Fe_2O_3t	5.62	5.41	3.26	4.04	3.90	3.63	3.83	3.53	2.26	3.72	1.42	2.39	2.41	1.72
Fe_2O_3	-	-	-	-	-	-	-	-	2.09	2.72	-	1.44	2.04	0.96
FeO	-	-	-	-	-	-	-	-	0.15	0.90	-	0.85	0.33	0.68
MnO	0.06	0.07	0.01	0.05	0.04	0.02	0.04	0.02	0.02	0.03	0.02	0.03	0.06	0.01
MgO	2.55	2.09	0.37	1.51	1.79	1.02	0.61	0.88	0.18	0.4	0.43	0.41	0.25	0.57
CaO	6.32	5.93	2.45	2.62	2.74	3.02	2.59	2.26	1.97	2.22	3.86	2.18	2.02	1.98
Na_2O	3.39	3.36	2.06	3.15	3.18	3.31	2.53	2.93	1.95	2.95	4.01	5.11	4.49	5.1
K_2O	3.6	3.28	7.33	3.92	3.86	4.02	5.11	5.17	8.37	5.61	1.89	2.17	2.8	2.48
P_2O_5	0.31	0.32	0.18	0.15	0.16	0.12	0.15	0.13	0.16	0.12	0.07	0.07	0.12	0.11
LOI	7.1	6.13	3.07	3	3.1	3.09	3.3	2.97	3.51	2.61	5.52	4.36	3.68	3.97
Total	100.1	99.71	99.15	99.29	99.76	99.43	99.75	99.27	99.77	100.12	99.37	99.25	99.48	99.15
Rb	134	125	163	135	134	146	157	150	-	-	44	-	-	-
Ba	655	650	653	494	520	630	521	600	-	-	442	-	-	-
Sr	578	502	342	265	275	289	239	250	-	-	455	-	-	-
Th	4.5	4.1	4.1	3.8	3.8	4.3	4	3.9	-	-	2.5	-	-	-
U	1	2	2	2	1	1	2	2	-	-	2	-	-	-
Pb	2	2	2	2	2	2	2	2	-	-	2	-	-	-
Zr	298	288	202	214	219	214	191	214	-	-	151	-	-	-
Hf	4	4	2	3	3	3	1	3	-	-	2	-	-	-
Nb	5	5	5	5	5	5	5	5	-	-	5	-	-	-
La	45	41	41	38	38	43	40	39	-	-	25	-	-	-
Ce	80	80	79	69	75	77	75	77	-	-	52	-	-	-
Nd	33	35	30	25	27	27	27	24	-	-	9	-	-	-
Y	20	20	13	16	16	17	16	16	-	-	-	-	-	-
Cr	110	111	37	54	56	52	54	49	-	-	4	-	-	-
Co	18	19	9	13	13	9	11	10	-	-	-	-	-	-
Ni	41	54	20	25	25	23	32	23	-	-	-	-	-	-
V	110	97	69	65	69	58	53	55	-	-	7	-	-	-
Cu	36	-	-	-	-	-	-	-	-	-	-	-	-	-
Zn	58	37	28	52	57	45	49	49	-	-	35	-	-	-
Mg #	0.961	0.816	0.234	0.777	0.953	0.581	0.330	0.515	0.162	0.223	0.610	0.350	0.212	0.671

Table 1. *Cont.*

No Fac.	**3**	**3**	**3**	**3**	**3**	**3**	**3**	**3**	**3**	**3**	**3**	**3**	**4**	**4**
No Samp.	**W147 ***	**YK4**	**W144 ***	**YK13**	**YK19**	**YK7**	**YK8**	**YK5**	**W182 ***	**W145 ***	**YK12**	**ARM15**	**YK14F**	**YK36F**
SiO_2	69.1	69.55	69.76	69.8	69.95	70.3	70.3	70.42	70.45	70.7	70.81	71.69	70.06	70.29
TiO_2	0.24	0.23	0.29	0.23	0.23	0.25	0.25	0.23	0.31	0.54	0.23	0.26	0.24	0.23
Al_2O_3	15.35	15.07	15.5	15.17	15.29	15.41	15.27	15.25	14.05	13.72	15.33	15.58	14.72	14.73
Fe_2O_3t	1.73	1.5	1.63	1.47	1.53	1.68	1.39	1.5	2.40	1.44	1.48	-	1.62	1.61
Fe_2O_3	1.36	-	1.07	-	-	-	-	-	2.08	0.18	-	1.63	-	-
FeO	0.33	-	0.5	-	-	-	-	-	0.29	1.13	-	-	-	-
MnO	0.03	0.01	0.03	0.02	0.01	0.02	0.02	0.01	0.04	0.02	0.01	0.03	0.03	0.03
MgO	0.7	0.43	0.45	0.43	0.42	0.11	0.18	0.43	0.26	0.61	0.44	0.21	0.7	0.7
CaO	2.55	2	1.12	1.93	1.83	1.85	1.92	1.94	0.49	1.93	1.76	0.19	1.88	1.87
Na_2O	4.11	4.11	4.38	4.12	4.21	4.72	4.33	4.11	4.85	4.75	4.14	3.75	4.11	4.11
K_2O	0.27	2.6	2.49	2.57	2.5	2.74	2.79	2.61	2.48	2.24	2.54	3.76	1.83	1.82
P_2O_5	0.07	0.07	0.08	0.07	0.07	0.07	0.07	0.07	0.11	0.08	0.07	0.12	0.05	0.05
LOI	5.51	3.45	3.6	3.31	3.2	2.69	3.1	3.34	3.33	2.91	3.22	1.98	4.15	4.07
Total	99.62	99.02	99.27	99.12	99.24	99.84	99.62	99.91	98.74	98.81	100.03	99.20	99.39	99.51
Rb	-	55	-	55	54	59	63	55	-	-	55	56.54	56	56
Ba	-	668	-	636	618	538	751	698	-	-	595	627.54	65	630
Sr	-	373	-	376	373	382	428	380	-	-	370	343.00	492	494
Th	-	2.7	-	2.6	2.7	2.7	2.6	2.9	-	-	2.7	3.69	2.9	2.7
U	-	2	-	2	2	2	2	2	-	-	2	0.63	2	2
Pb	-	2	-	2	2	2	2	2	-	-	2	30.93	2	2
Zr	-	153	-	156	156	153	155	157	-	-	158	183.00	153	155
Hf	-	2	-	2	2	2	2	2	-	-	2	3.60	2	2
Nb	-	5	-	5	5	5	5	5	-	-	5	2.21	5	5
La	-	27	-	26	27	27	26	29	-	-	27	20.45	29	27
Ce	-	49	-	50	54	48	48	43	-	-	49	37.85	52	51
Nd	-	8	-	7	13	13	10	9	-	-	9	15.58	14	12
Y	-	-	-	-	-	-	-	-	-	-	-	4.64	-	-
Cr	-	2	-	1	1	3	2	10	-	-	3	-	1	-
Co	-	-	-	-	-	-	-	-	-	-	-	-	-	-
Ni	-	-	-	-	-	-	-	-	-	-	-	23.00	-	-
V	-	9	-	11	9	14	12	12	-	-	11	-	9	11
Cu	-	-	-	-	-	-	-	-	-	-	-	-	-	-
Zn	-	15	-	13	13	38	98	14	-	-	16	-	76	76
Mg #	0.819	0.578	0.559	0.589	0.554	0.132	0.261	0.578	0.221	0.855	0.599	-	0.872	0.878

Table 2. SHRIMPII zircon U–Th–Pb results of the rhyolitic dome of TSESDAI.

Unit/ Sample	Spot Name	Concentrations						Ratios									Ages (Ma)				Conc %
		U (ppm)	Th (ppm)	$^{232}Th/^{238}U$	± %	$^{206}Pb^*$ (ppm)	^{206}Pbc (%)	$^{238}U/^{206}Pb^*$	1 σ %	$^{207}Pb^*/^{206}Pb^*$	1 σ %	$^{207}Pb^*/^{235}U$	1 σ %	$^{206}Pb^*/^{238}U$	1 σ %	Rho	$^{206}Pb/^{238}U$	1 σ (Ma)	$^{207}Pb/^{206}Pb$	1 σ (Ma)	
Tiddas Souk Es-Sebt Des Ait Ikko/Ari el Mahsar/ARM15	1.1	283	171	0.62	2.31	20.3	0.30	11.945	3.468	0.0594	0.991	0.69	3.607	0.084	3.468	0.962	518	17	582	22	111
	2.1	615	365	0.61	1.59	24.2	−0.02	21.851	3.083	0.0519	0.721	0.33	3.166	0.046	3.083	0.974	288	9	282	16	98
	3.1	632	468	0.76	0.78	23.4	0.56	23.206	3.121	0.0538	1.527	0.32	3.474	0.043	3.121	0.898	272	8	362	34	125
	4.1	675	383	0.59	1.34	25.3	0.15	22.856	3.055	0.0522	0.904	0.32	3.186	0.044	3.055	0.959	276	8	295	21	107
	5.1	619	260	0.43	4.79	24.0	0.14	22.116	3.053	0.0529	0.807	0.33	3.158	0.045	3.053	0.967	285	9	323	18	112
	6.1	497	219	0.46	0.69	47.1	4.08	8.711	3.447	0.0941	0.508	1.49	3.484	0.115	3.447	0.989	701	23	1510	10	157
	7.1	399	169	0.44	0.22	16.1	0.16	21.211	3.237	0.0525	1.400	0.34	3.527	0.047	3.237	0.918	297	9	309	32	104
	8.1	165	97	0.60	0.66	64.5	1.21	2.174	3.087	0.1669	0.285	10.59	3.101	0.460	3.087	0.996	2439	63	2527	5	104
	8.2	669	380	0.59	0.22	25.5	0.23	22.522	3.063	0.0520	1.496	0.32	3.409	0.044	3.063	0.899	280	8	284	34	101
	9.1	564	744	1.36	0.49	41.8	0.80	11.541	3.057	0.0606	1.227	0.72	3.294	0.087	3.057	0.928	536	16	625	26	115
	10.1	229	50	0.23	1.47	49.8	1.37	3.902	3.165	0.1030	0.784	3.64	3.260	0.256	3.165	0.971	1471	42	1679	14	114
	10.2	484	160	0.34	2.51	47.3	2.26	8.583	3.371	0.0809	0.722	1.30	3.448	0.117	3.371	0.978	710	23	1219	14	144
	11.1	557	323	0.60	0.71	22.0	0.56		3.223	0.0527	1.871	0.33	3.727	0.046	3.223	0.865	290	9	318	43	109
	11.2	176	86	0.50	9.59	10.1	0.31	14.943	4.013	0.0588	2.546	0.54	4.753	0.067	4.013	0.844	418	16	561	55	126
	12.1	582	387	0.69	0.83	23.2	0.35	21.585	3.531	0.0516	1.963	0.33	4.039	0.046	3.531	0.874	292	10	267	45	90
	13.1	195	81	0.43	0.65	39.9	2.04	4.114	3.089	0.1055	0.495	3.53	3.129	0.243	3.089	0.987	1403	39	1722	9	121
	13.2	652	332	0.53	0.73	26.2	0.18	21.409	3.143	0.0520	1.543	0.33	3.501	0.047	3.143	0.898	294	9	284	35	96
	14.1	497	171	0.36	0.41	28.9	0.14	14.786	3.937	0.0556	2.050	0.52	4.439	0.068	3.937	0.887	422	16	438	46	104
	14.2	105	56	0.55	0.39	8.3	0.55	10.896	3.138	0.0589	2.984	0.74	4.330	0.092	3.138	0.725	566	17	562	65	99
	15.1	243	116	0.49	0.29	11.7	0.54	17.881	3.087	0.0548	2.342	0.42	3.875	0.056	3.087	0.797	351	11	402	52	113
	16.1	300	139	0.48	0.27	24.2	0.07	10.638	3.133	0.0603	0.876	0.78	3.254	0.094	3.133	0.963	579	17	616	19	106
	17.1	471	186	0.41	0.81	19.5	0.58	20.707	3.190	0.0541	2.456	0.36	4.026	0.048	3.190	0.792	304	9	376	55	120
	18.1	336	104	0.32	0.55	29.2	0.09	9.864	3.072	0.0611	0.754	0.85	3.163	0.101	3.072	0.971	622	18	644	16	104
	19.1	49	52	1.10	0.46	4.1	0.39	10.235	3.248	0.0609	3.219	0.82	4.573	0.098	3.248	0.710	601	19	637	69	106
	19.2	440	186	0.44	2.01	17.0	0.87	22.216	3.150	0.0521	4.986	0.32	5.897	0.045	3.150	0.534	284	9	290	114	102
	20.1	361	4	0.01	1.34	101.3	1.44	3.023	3.071	0.1235	0.307	5.63	3.086	0.331	3.071	0.995	1842	49	2007	5	125
	20.2	1129	410	0.37	0.35	71.3	1.01	13.605	3.706	0.0566	4.970	0.57	6.199	0.074	3.706	0.598	457	16	475	110	104
	21.1	774	478	0.64	0.19	31.6	0.14	21.065	3.058	0.0522	1.213	0.34	3.290	0.047	3.058	0.930	299	9	294	28	98
	22.1	461	45	0.10	2.34	112.5	2.73	3.424	3.063	0.1227	0.274	4.94	3.075	0.292	3.063	0.996	1652	45	1996	5	120
	22.2	1082	920	0.88	0.19	40.7	0.14	22.807	3.162	0.0517	1.283	0.31	3.413	0.044	3.162	0.927	277	9	273	29	99
	23.1	649	399	0.63	0.46	25.3	0.30	22.068	3.223	0.0520	1.643	0.33	3.618	0.045	3.223	0.891	286	9	287	38	101

Errors are 1-sigma; Pbc and Pb* indicate the common and radiogenic portions, respectively. Common Pb corrected using measured ^{204}Pb.

3.2.2. Whole-Rock Geochemistry

Chemical compositions of the analyzed whole rocks are given in (Table 1), which also presented nine whole rock chemical analyses available on the literature (identified by an asterisk; [19,28]). Whole rocks of 18 samples were analyzed for major oxides and trace elements by X-ray fluorescence (XRF) spectroscopy using a Phillips PW 1400 at the Centre d'Analyses Minérale, University of Lausanne, Lausanne, Switzerland. After reducing the sample to centimeter sized chips in a hydraulic press, the freshest pieces were selected and crushed using a jaw crusher and then powdered in an agate swing mill. Routine analyses of major elements and traces were performed on fused disks prepared from 1.2 g of calcined sample powder mixed with lithium-tetraborate. Calibrations were based on certified international standards. The limits of detection depend on the element concerned and the matrix but typically range between 1 to 7 ppm. The dated sample (ARM 15) was analyzed for bulk rock major and trace element analyses using the analytical facilities of the Instituto Andaluz De Ciencias De La Tierra (IACT), CSIC–UGR, Armilla, Granada, Spain. The analytical techniques were described in detail by [42].

3.2.3. Mineral Chemistry: Electron Probe MicroAnalyser (EPMA)

Major and trace element analyses of minerals (pyroxenes and biotites) were performed at the CAMP-Paris of the University of Pierre et Marie Curie (Laboratoire de Géochimie Comparée et Systématique, Paris, France) using a Cameca SX100 electron microprobe calibrated with a combination of natural and synthetic standards including sanidine (Al), titanite (Ti, Si, and Ca), halite (Cl), chromite (Cr), topaz (F), andradite (Fe), orthoclase (K), olivine (Mg), spessartine (Mn), and albite (Na). Analyses were carried out using a beam size of 1 µm, an accelerating voltage of 15 kV, and a probe current of 20 nA. Counting time varied depending on elements and minerals (see [38] for more details).

4. Results

4.1. Field Observations and Petrographic Features

The major types of volcanic rocks outcropping in the TSESDAI basin and their petrographic features are summarized below.

4.1.1. Dolerites

These rocks crop out in the northeastern sector of the Tiddas region as a NE–SW kilometric length dolerite dike (50 m thick). Their primary mineralogical composition consists of pyroxene and plagioclase (60–70% An), both presenting variable degrees of alteration. Pyroxene are often epigenized into secondary minerals such as chlorite, calcite, and silica, while plagioclases are partially or completely sericitized.

4.1.2. Sebt Ait Ikko Andesites

The andesites crop out southwest of Sebt Ait Ikko, on both sides of the Oued BouAzza valley. They consist of a 15 m thick flow pile uncomfortably resting on the F1 formation of Permian detrital deposits [38]. These andesites are mainly composed of plagioclase, pyroxene, and olivine, presenting variable degrees of alteration.

4.1.3. Tiddas Andesites and Associated Pyroclastites

In the vicinity of Tiddas, the andesites and associated pyroclastites crop out at the Kikene and Glimis Mountains (Figure 3A). They consist of 15 to 50 m thick flows and pyroclastites lying with an angular unconformity directly on the Visean basement [38]. The summit is systematically underlined by metric-scale horizons of breccias, sometimes covered by tuffs of ash lapillis of the same nature and Permian detritic deposits of the F1 formation. The mineralogical assemblage essentially consists of pyroxenes and plagioclases.

Figure 3. Field photographs: (**A**) Tiddas andesites located to the SW of this village; (**B**) dacites of Bled Bou Haouza located to the SE of Sebt Ait Ikko; (**C**) Ari el Mahsar dome laying on the Visean basement; (**D**) a close view of the rhyolites in the Ari el Mahsar dome. The location of sample ARM15 is indicated.

4.1.4. Pyroxenes Dacites

These rocks outcrop exclusively in the area of Bled Bou Haouza (Figure 3B). They are either laying directly or with an angular discordance over the folded or laminated upper Visean basement. Occasionally they are separated from the latter by Autunian molasses formed conglomeratic and sandstone deposits with mainly F1 volcanic elements. Sometimes, they are overlain by a level of breccias of the same nature. The mineralogical assemblage is composed of pyroxene, plagioclase, and sanidine.

4.1.5. Biotite Rhyolites

The biotite rhyolites outcrop in the eastern part of TSESDAI as extrusive domes associated with a network of rhyolitic dikes with a NE–SW general trend. The dome and the dikes are both systematically intrusive in the pre-Permian basement. The rhyolitic domes (Figure 3C,D) have generally prismatic joints, developing vertical prisms of about 15 to 20 m in height. Sometimes the prisms are imperfect as a result of the development of horizontal joints. The prismatic feature locally disappears due to the latter development of spheroidal disjunction. The rhyolitic dikes have a general trend of N50–60 and a metric to kilometer extension, with frequent columnar jointing with contiguous sharp edge columns characterized by centimetric polygonal sections. Massive, rounded blocks with "onion peel" structures are common.

4.1.6. Lapilli Tuffs and Rhyolitic Ash Deposits

These 5 m thick lenticular pyroclastic deposits are interbedded within the detrital deposits of the formation F1. They are characterized by a decimetric stratification with internal horizontal laminations, normally or inversely graded, with occasional accretionary lapilli levels.

4.2. Lithostratigraphic Organization

Figure 4 illustrates the spatiotemporal distribution of the described facies. Depending on the areas, 50 to 350 m thicknesses of sedimentary, lava flows, and pyroclastic deposits

have been accumulated, representing about 24 km^3 of the volcanic and sedimentary material. The buildup of these piles is the result of a volcanological and sedimentary evolution that differs very little from one sector to another. The standard volcanic succession includes (i) a 15 to 50 m thick stack of andesites breccias (Tiddas andesites), castings and lapilli tuff, and andesitic ash deposits; (ii) 100 m of rhyolitic lavas structured in a series of domes and preceded by the intrusion of rhyolitic dikes, a phase that forms stratigraphically and that is the lateral equivalent of the "Tiddas andesites"; (iii) 2 m deposits of lapilli tuffs and rhyolitic ashes that are contemporaneous with the filling of the basin (deposits of the F1 formation); (iv) 60 m of flows and breccias of dacite; (v) 15 m of andesite flows; and (vi) 50 m of basaltic flows.

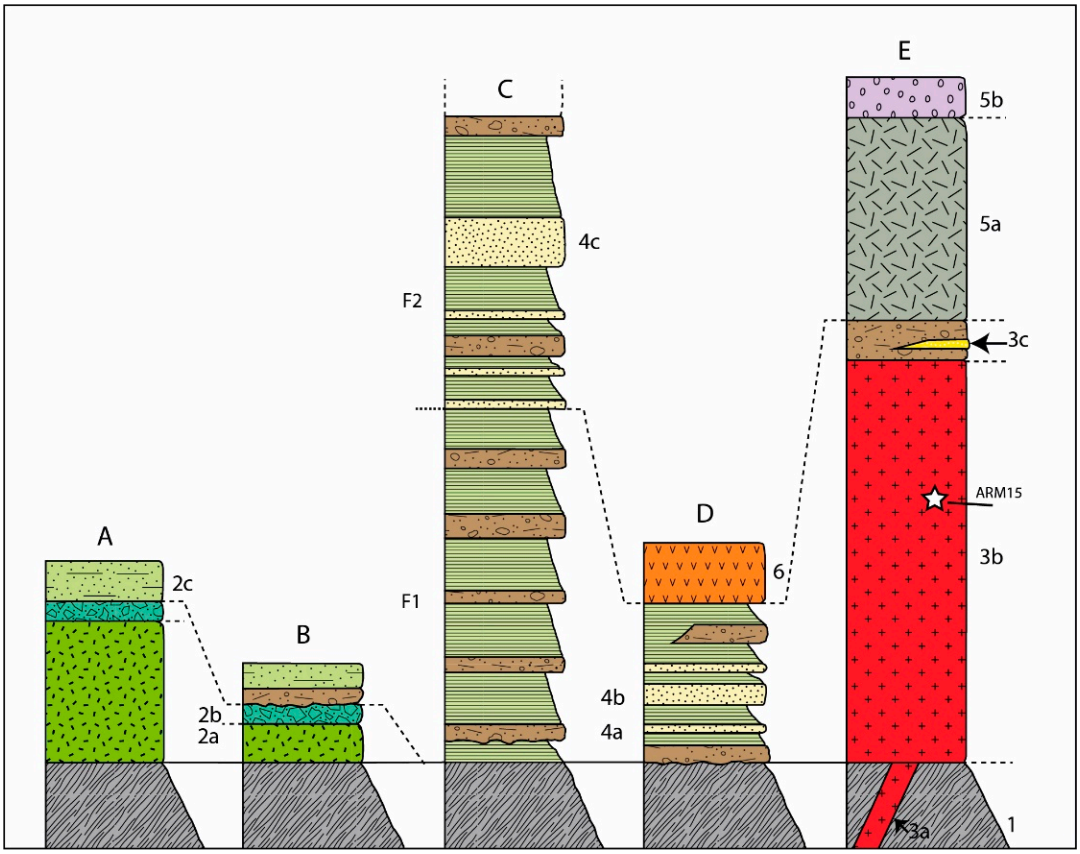

Figure 4. Lithostratigraphic columns of the Permian volcanic complex of TSESDAI: 1. Upper Visean Paleozoic terrains; 2. Tiddas pyroxene andesites in flows (2a), flow breccias (2b), and lapilli tuff and ash deposits (2c); 3. biotite rhyolitic dikes (3a), domes (3b), and lapilli tuffs and ash deposits (3c); 4. detrital formations of Permian conglomerates (4a), argillites (4b), and sandstones (4c); 5. Bled Bou Haouza dacites with pyroxenes (in flows (5a) and flow breccias (5b); 6A Sebt Ait Ikko andesites with olivine and pyroxenes. F1, lower formation; F2, intermediate formation. Location of sections; (**A**), west of Tiddas (Glimis); (**B**), west–southwest of Tiddas (KiKene); (**C**), northeast of Tiddas; (**D**), southwest of Sebt Ait Ikko; (**E**), south of Sebt Ait Ikko.

4.3. Mineral Chemistry

4.3.1. Clinopyroxenes of Dacites

The clinopyroxenes (Cpx) are colorless with polysynthetic twins and/or sectorial zoning structures constituting 5% of the total volume of the dacitic lava flows. They appear as phenocrysts (2%) and microlites (3%) (Figure 5A) and are euhedral or subhedral, sometimes corroded. Cationic proportions based on six oxygen atoms per formula unit of the studied clinopyroxenes allowed them to be classified mainly as augites, using [43] systematics, with compositions clustered around an average of En 42–Wo 42–Fs 16 (Figure 6, Tables S1 and S2). They are characterized by (i) a high SiO_2 content (49.66 wt.% up to 52.66 wt.% and an average of 51.22 wt.%); (ii) a low TiO_2 content (0.31 up to 1.70 wt.% with

an average of 0.60 wt.%; (iii) a low or high Al_2O_3 content (1.04 to 5.5 wt.% with an average of 2.09 wt.%); (iv) and a CrO_3 content ranging from 0.025 to 0.31 wt.% with an average of 0.10 wt.%. Al^{IV} is usually low (0.034 to 0.141) indicating the lack of significant non-quadrilateral substitutions. These are accomplished by the incorporation of small amounts of aluminum (Al^{VI} = 0 to 0.101) and titanium (Ti = 0.009 to 0.048) in the octahedral site.

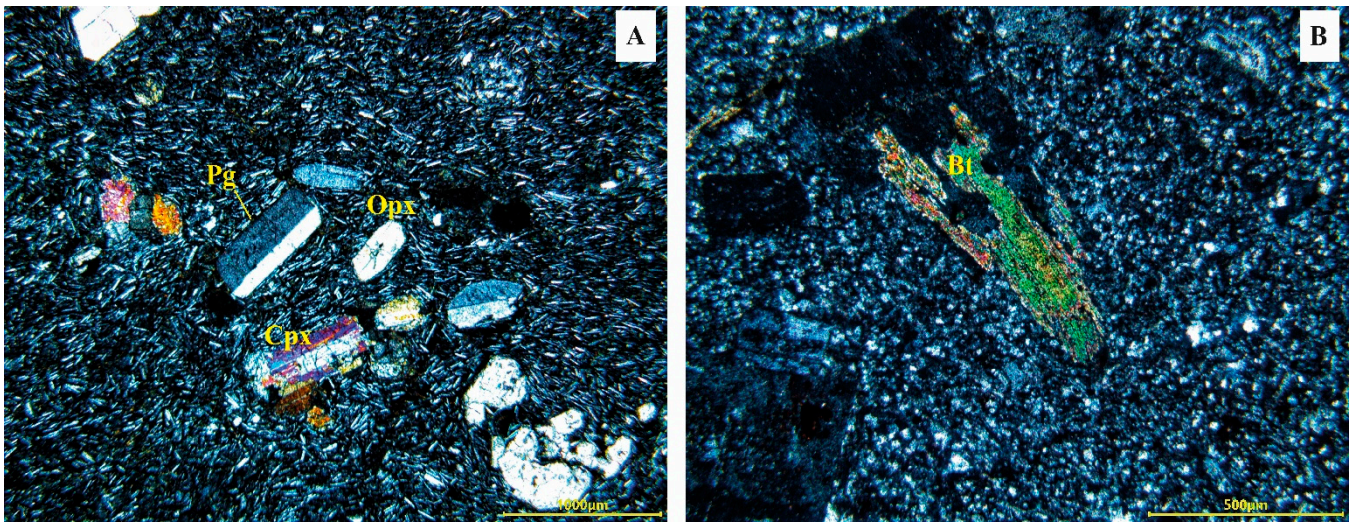

Figure 5. Thin-section photomicrographs of andesites from Tiddas and the ARM 15 sample. (**A**) Tiddas andesite with plagioclase (Pl), clinopyroxene (Cpx), and orthopyroxene (Opx); (**B**) sample ARM15 of a rhyolitic dome with biotites (Bt).

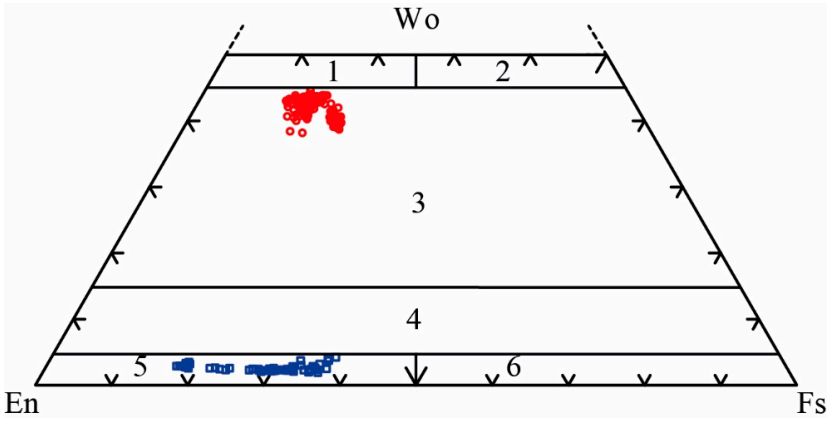

Figure 6. Pyroxene composition of the dacite flows of the TSESDAI eruptive complex in the enstatite (En), Wollastonite (Wo), and ferrosilite (Fs) triangle of [43]. Blue circles indicate the analyzed orthopyroxenes. Red circles indicate the analyzed clinopyroxenes. The numbers (1 to 6) indicate respectively; Diopside, Hedenbergite, Augite, Pigeonite, Clinoenstatite, Clinoferrosilite.

4.3.2. Biotite of Rhyolites

Biotite constitutes about 6% of the total rock volume and appears isolated or grouped in glomeruli with feldspar phenocrysts (2%) being euhedral to subhedral with rarely corroded contours (Figure 5B), and as microlites (4%). Biotite crystals retain generally their primary optical characteristics, but occasionally they are partially or totally transformed into chlorite and invaded by oxide granules (Figure 5B). The chemical analyzes of the biotites and their structural formulas calculated on the basis of 22 oxygen atoms (Table S3) show that they are characterized by (i) low iron oxide content (mean average = 17.45 wt.%) and calcium (CaO = 0.09 wt.%); (ii) relatively high levels of titanium (TiO_2 = 3.13 wt.%), which is compatible with a medium magmatic formation, alumina (Al_2O_3 = 15.28 wt.%), and magnesium (MgO = 11.72 wt.%) (e.g., [44–47]; and (iii) Fe/Mg + Fe ratios ranging between 0.44 and 0.49 allowing their classification as magnesian biotites (see Figure 7; [48]).

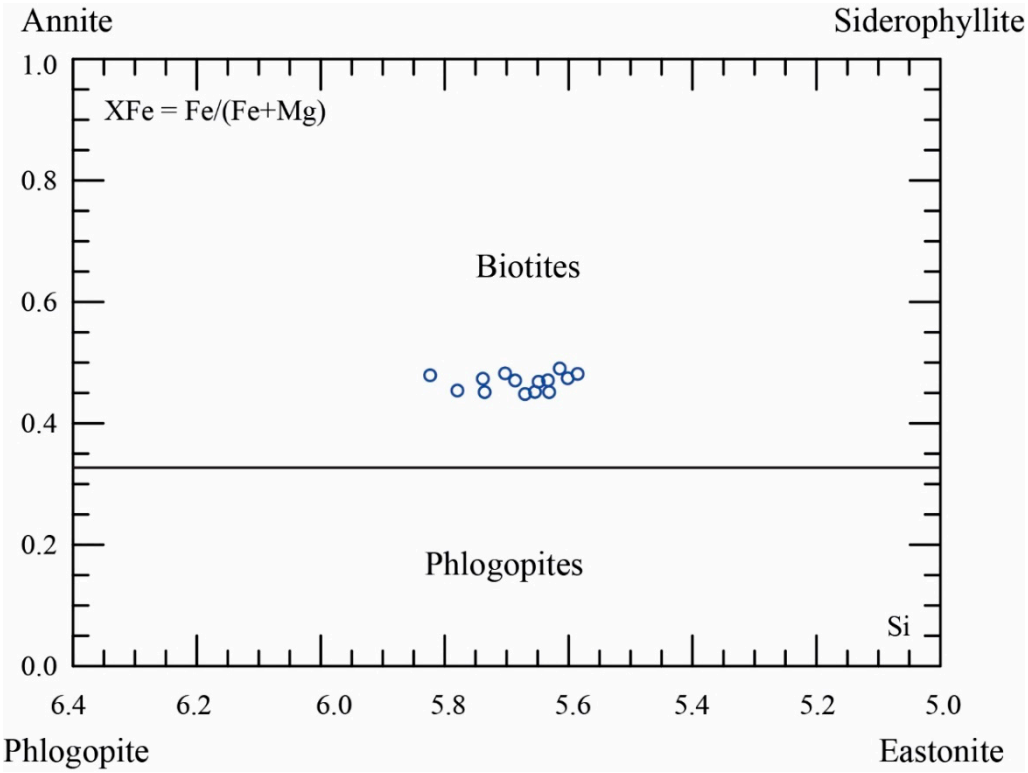

Figure 7. Biotite's compositional domain of the TSESDAI rhyolitic dome in the Fe/Fe + Mg diagram of [48]. Blue circles indicate the analyzed Biotites.

4.4. Whole-Rock Geochemistry

4.4.1. Major Elements

The studied volcanic and subvolcanic rocks display variable contents of SiO_2 (54.11 to 70.80 wt.%), Al_2O_3 (13.42 to 15.99 wt.%), CaO (0.49 to 6.32 wt.%), MgO (0.11 to 2.55 wt.%), and alkalis ($Na_2O + K_2O$ = 4.38 to 10.32 wt.%). Loss on ignition (LOI) contents are moderately high and variable (LOI = 1.98 to 6.13 wt.%) suggesting the operation of post-magmatic processes, which requires caution when interpreting the concentrations of the more mobile elements (e.g., alkalis). The classification diagram of [49] shows that the studied rocks occupy the fields of basaltic trachyandesite, trachydacites, and rhyolites. The rhyolites (in domes and dikes) from TSESDAI display a sub-alkaline behavior, while the andesites and dacites display an alkaline one [50] (Figure 8). The andesites and a large part of the dacites have a very high K_2O content due to the alteration of feldspar to sericite. This explains the migration of their representative points in domains not identical to those indicated by their petrographic and mineralogical features, and this is mainly due to the alteration of feldspar to sericite and clays and devitrification glasses made up of chlorite and other clay minerals. The evolution diagram of [51] (Figure 9), where the content of SiO_2 is taken as an index of differentiation, allows for the following remarks:

- The TiO_2, Al_2O_3, FeO*, MgO, CaO, and P_2O_5 oxides have a negative correlation with SiO_2, while K_2O and Na_2O have an opposite or a random behavior.
- A negative correlation of Al_2O_3 and SiO_2 in the dacitic terms could be a result of the fractionation of alumino-silicate minerals such as plagioclase. The same correlation is observed in the transition from dacites to rhyolites.
- The occurrence of a hiatus between the mafic terms (andesites), the intermediate and the felsic terms (dacites and rhyolites). The intermediate terms of the felsic andesite type are absent.

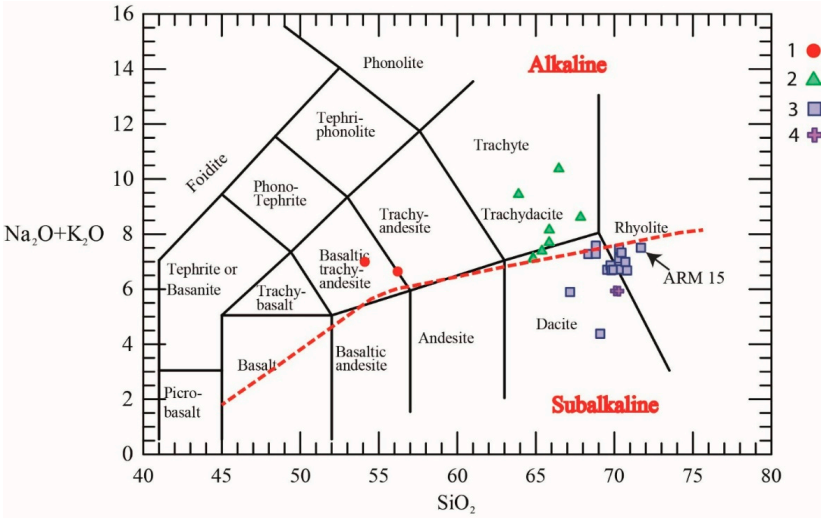

Figure 8. Chemical nomenclature of the volcanic rocks of the TSESDAI eruptive complex. Legend: (1) andesites; (2) dacites (Bled Bou Haouza); (3) rhyolitic domes; (4) rhyolitic dike.

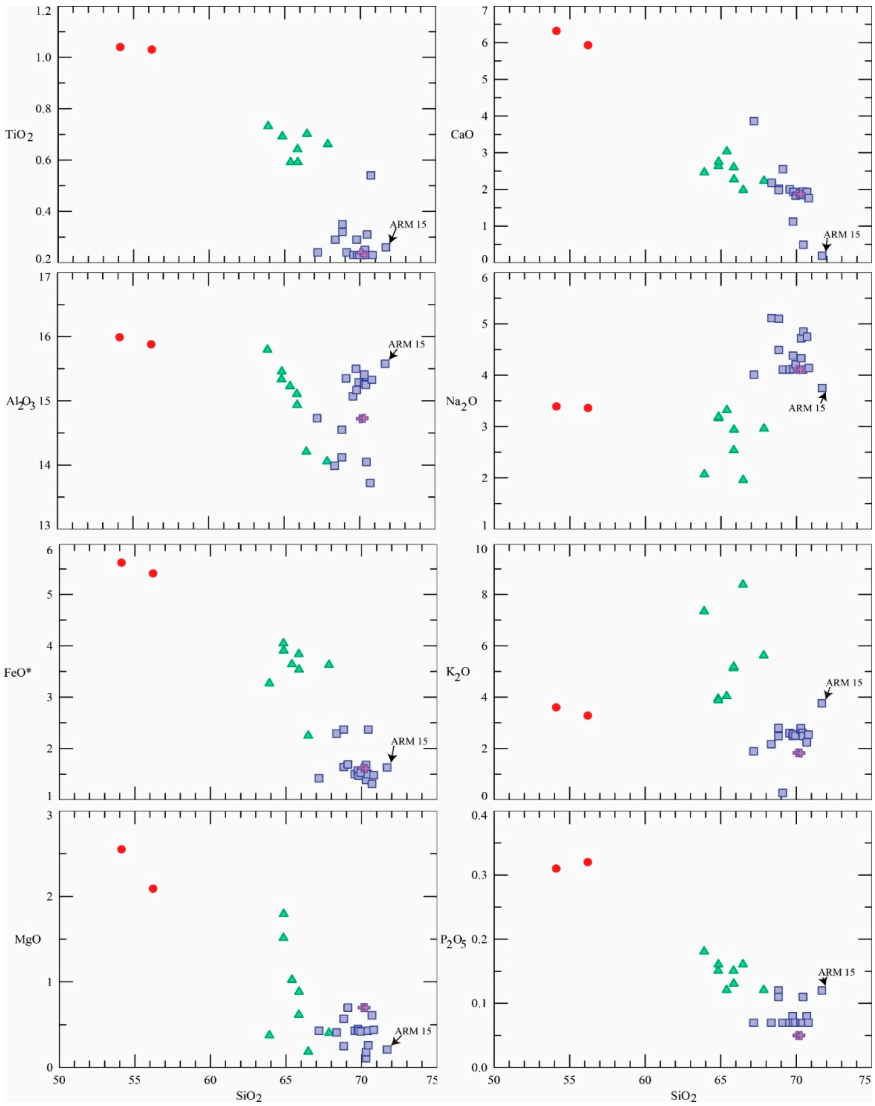

Figure 9. Diagrams of the variation of some oxides versus SiO_2. See symbol legend in Figure 8.

4.4.2. Trace Elements

The contents of large-ion lithophile element (LILE) including low field strength (LFS) (Rb, K, Ba, Sr, Th) and light rare earth elements (La, Ce) occasionally display large variations. However, the same order of magnitude for the various facies and for a given element is preserved. The behavior of Sr seems compatible with plagioclase fractionation in the andesite–dacite series (Figure 10) (correlation between CaO and SiO_2 in these rocks). Ba shows a slightly positive correlation with SiO_2 in andesites. The decrease of Ba in dacites and rhyolites is related to the fractionation of Ba-rich minerals such as Sanidine. The Th and rare earths (e.g., La, Ce, Nd) have a negative correlation with SiO_2 (Figure 10).

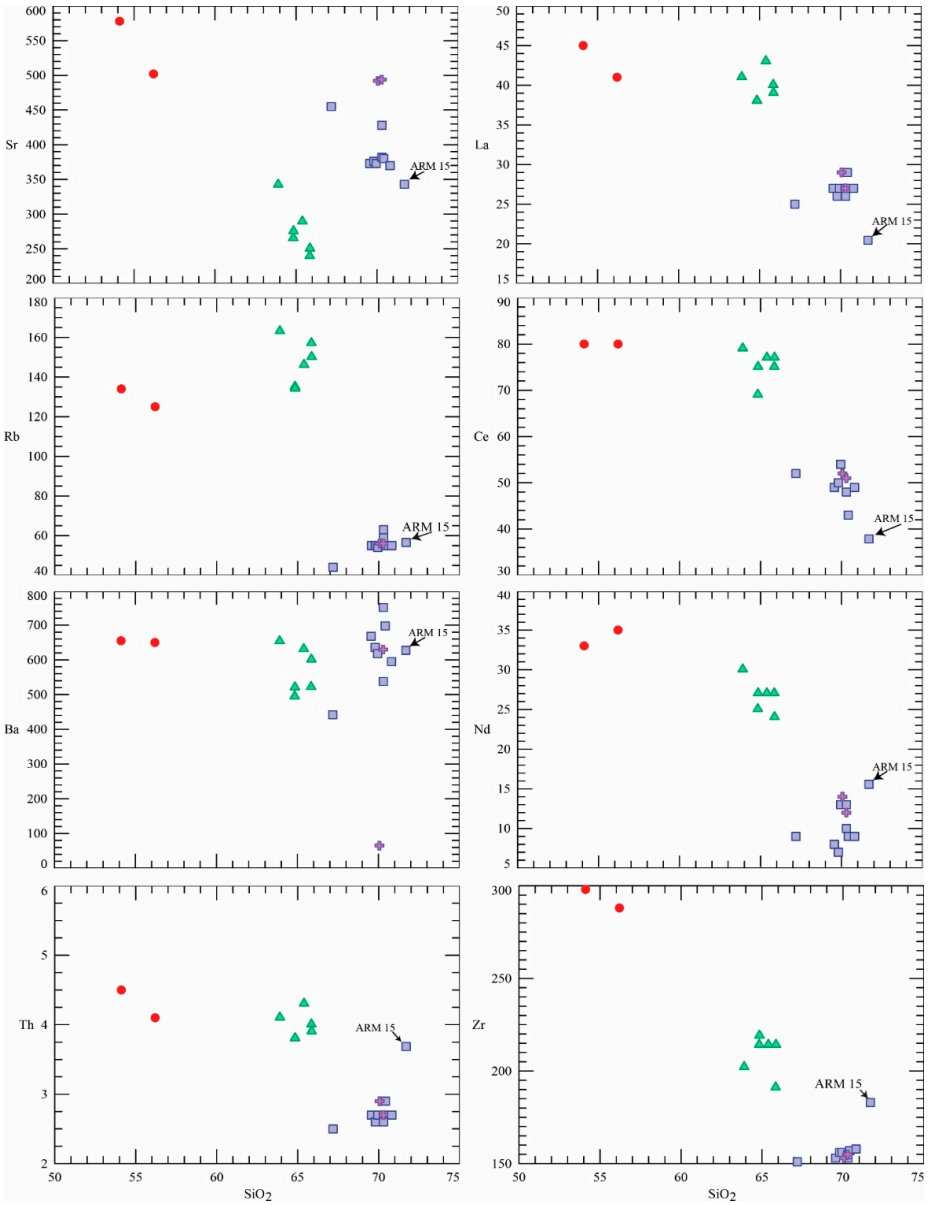

Figure 10. Diagram of the variation of some trace elements versus SiO_2. See symbol legend in Figure 8.

The high field strength elements (HFSE), such as Zr, Hf, Ti, P, Nb, and Ta are considered immobile during the alteration [52–54]. In the studied volcanic and subvolcanic facies, Zr and Hf contents are also high. The Zr contents range between 151 to 298 and the Hf contents vary from 1 to 4. The latter shows a negative correlation with SiO_2. The spectra obtained for andesites and dacites (Figure 11A), although corresponding to rocks of

different mineralogical compositions and degrees of differentiation, have very similar traces, when compared to MORB N, all these profiles presenting important enrichments in strongly incompatible elements (LILE), an important decrease between Th and Y (Th/Y = 0.56 to 0.84, average = 0.66), with a well-marked negative anomaly in Nb and a depletion in Ti and transition elements of the 3d series; in addition, the values of the La/Nb ratios are between 2 and 7 (La/Nb = 2.93 to 4.3, average 3.73). Compared to the andesites, the dacites show more pronounced negative TiO_2 and P_2O_5 anomalies, higher La/Th ratios, and a depletion of less incompatible elements, particularly the transition elements of the 3d series. Similarly, the LILE (Sr, Ba, Rb, U, Th) appear low in comparison to the Nb, La, and Ce contents. All the spectra of rhyolitic domes show, when compared to the ORG (Figure 11B), an enrichment in LILE (Sr, K, Rb, Ba, Th, La, and Ce), an increased deficit in weakly incompatible elements or HFSE (Zr, Hf, and Nb), with a significant decrease between Th and Nb that triggers a very marked negative anomaly in Nb (Th/Nb varies from 0.5 to 0.58 with an average of 0.54). An important fractionation of light rare earths is underlined in the Trace elements spidergram by the slope of the line between La and Nd (La/Nd varies from 2.07 to 3.71, average of 2.71) and the enrichment in LILE. The spectra of rhyolites when compared to the ORG shows Rb/Zr ratios very similar to those of [55], with values that go from 0.29 to 0.41, averaging 0.36.

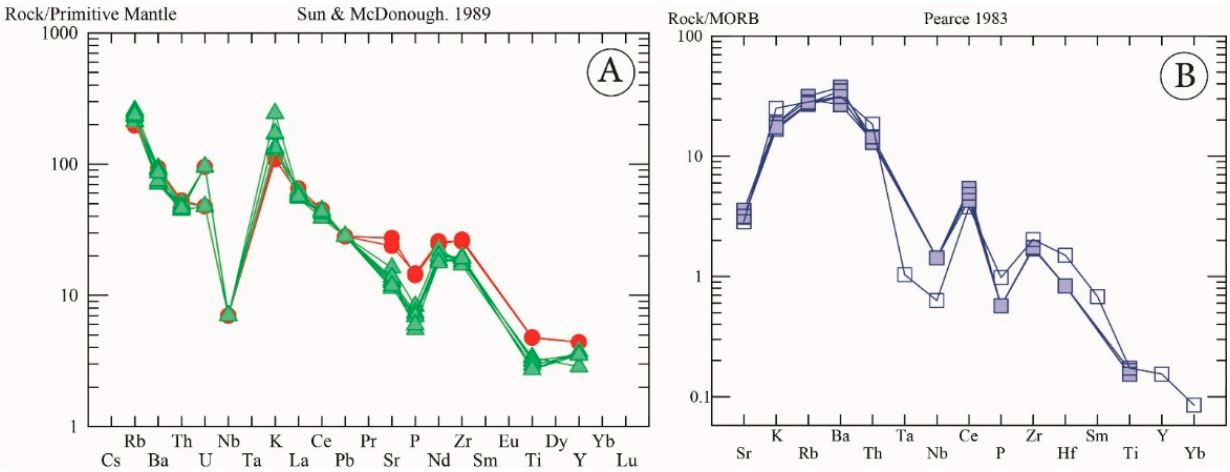

Figure 11. Trace elements spidergram of TSESDAI andesites and dacites normalized to N-type MORB (**A**), and of a TSESDAI rhyolitic dome normalized to ORG (**B**). See symbol legend in Figure 8.

4.5. Geochronology: The Shark Fin Rhyolitic Extrusive Dome of Ari el Mahsar, Sample ARM15

Zircons from sample ARM15 exhibit mean lengths and widths of 240 µm and 98 µm, respectively; they are euhedral to subhedral. Cathodo-luminescence images show oscillatory zoning patterns in most zircons. Some grains show an overgrowth by continuous non-luminescent rims with cores that are mostly zoned in an oscillatory manner, which can be interpreted as inherited (Figure 12). In addition, the morphological typology of the zircons shows the omnipresence of the S type around an S13 nucleus, the average points IA and IT [56], respectively, reaching values of 385 and 420, with formation temperatures between 750 °C and 800 °C (Figure 13). The Th/U ratio ranges from 0.01 to 1.36, indicating a mostly igneous population [57,58]. The Concordia diagram shows that the shark-fin-like rhyolitic extrusive dome of Ari el Mahsar (sample ARM15) yielded two predominant Concordia ages (603 ± 25 Ma and 286.4 ± 4.7 Ma) (Figure 14, Table 2). The young age is more concordant, being interpreted as the crystallization age of rhyolites, while the 603 Ma age indicates inherited zircon from the Pan-African crust under the Rehamna.

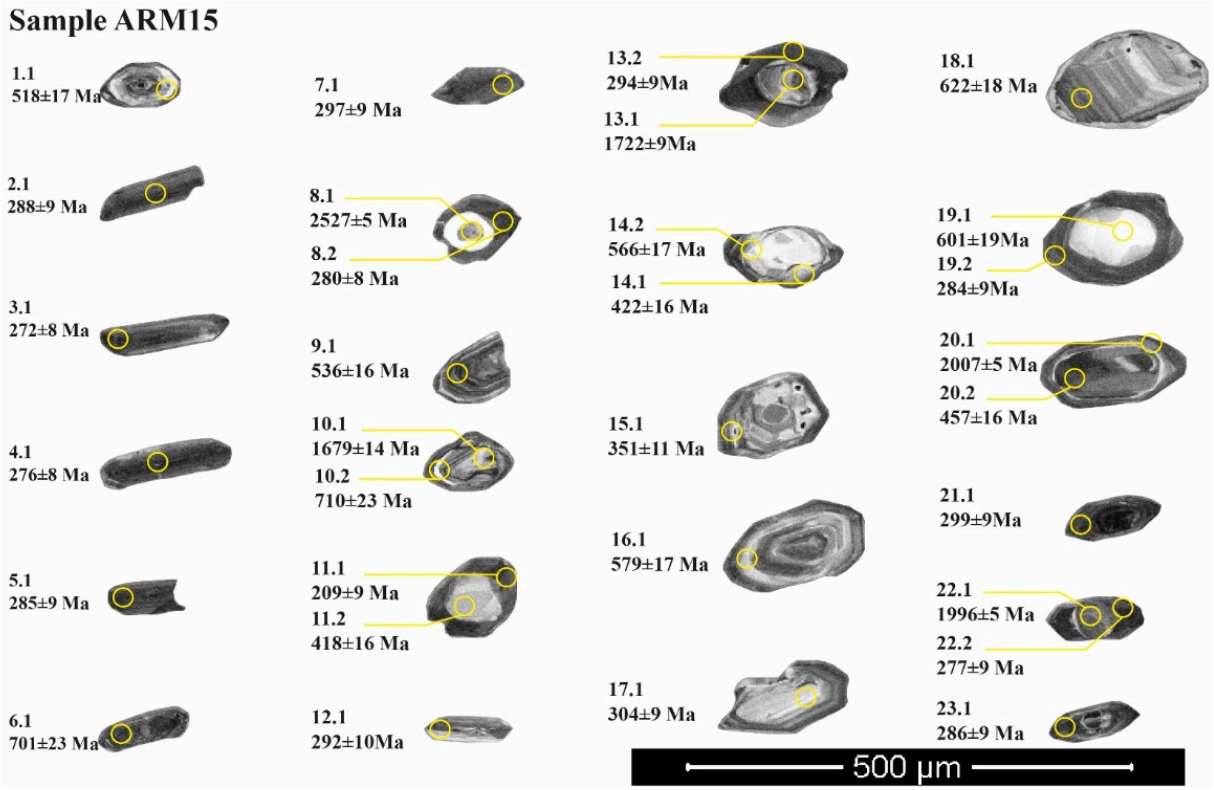

Figure 12. Cathodoluminescence (CL) images of zircon grains obtained from the rhyolitic sample (ARM15) showing their internal texture, spots (yellow circles), and apparent $^{206}Pb/^{238}U$ ages in Ma (1σ error).

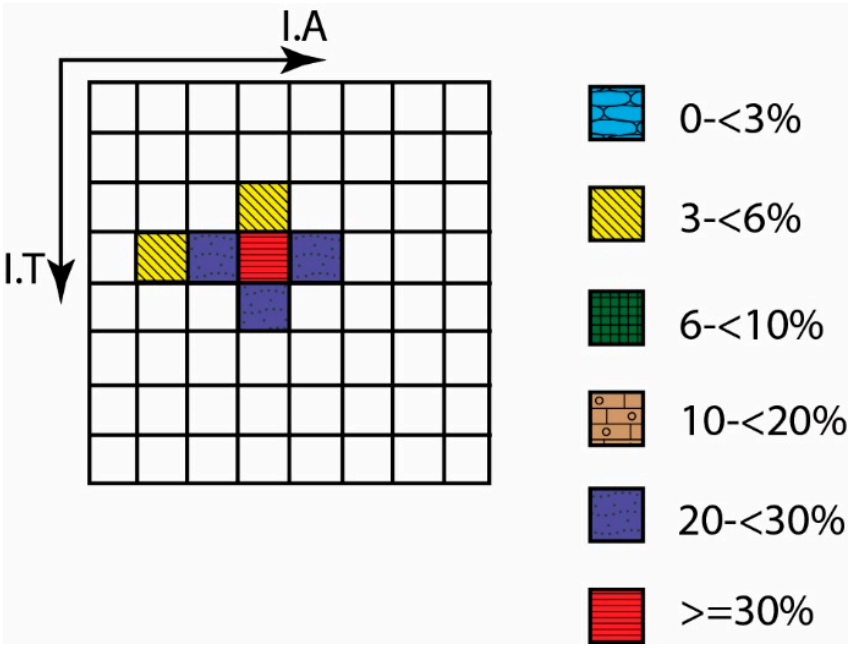

Figure 13. Typological distribution diagram of zircons from biotites of Ari el Mahsar rhyolitic dome.

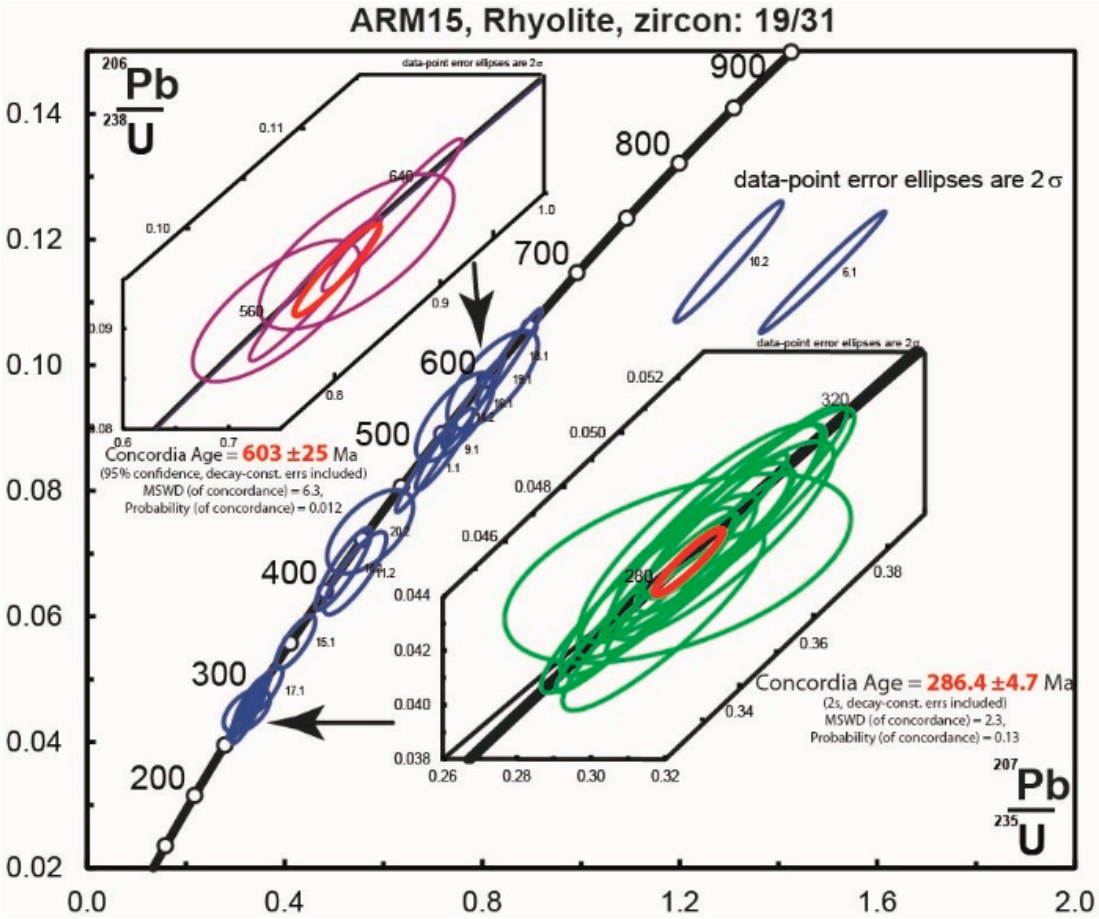

Figure 14. Zircon U–Pb SHRIMP geochronology. Wetherill Concordia plots of U–Pb zircon data for the rhyolitic sample (ARM15).

5. Discussion

5.1. The Calc-Alkaline Affinity of TSESDAI Rocks

Given the evidence for alteration of the studied rocks (LOI up to 6.13 wt.%), the use of alkali concentrations to decipher the magmatic affinities of the rocks was discarded. Instead, we used the ratio (Nb/Y) between two elements, which being characterized by high field strength are as such considered immobile during meteoric alteration and low-grade metamorphism and are also considered proxies of the degree of alkalinity of magmas (e.g., [59,60]). The studied rocks are characterized by Nb/Y ratios clearly below 0.6, the threshold usually considered as a divider between sub-alkaline and alkaline affinities, clearly pointing to the sub-alkaline characteristics of these rocks. Additionally, all the volcanic rocks of Tiddas show an absence of enrichment in FeO and TiO_2 with the increase of the magmatic evolution, as represented by the index FeO*/MgO, clearly pointing, according the criteria defined by [61,62], to the calc-alkaline characteristics of these rocks. This is confirmed by the low contents in TiO_2 (0.23 to 1.04%) and by the negative anomalies in Nb and Ti in the primordial mantle normalized diagrams (Figure 15) and by Zr/Y ratios clearly above 7 (see [59]). The chemical data collected on clinopyroxenes (cf. supra) confirm this calc-alkaline affinity with clinopyroxenes plotting on the calc-alkaline orogenic basalt field in the discrimination diagrams of [63] (Figure 15) and [64] (Figure 16). Additionally, the composition of biotites is typical from those usually found on calc-alkaline rocks (Figure 17; [46]).

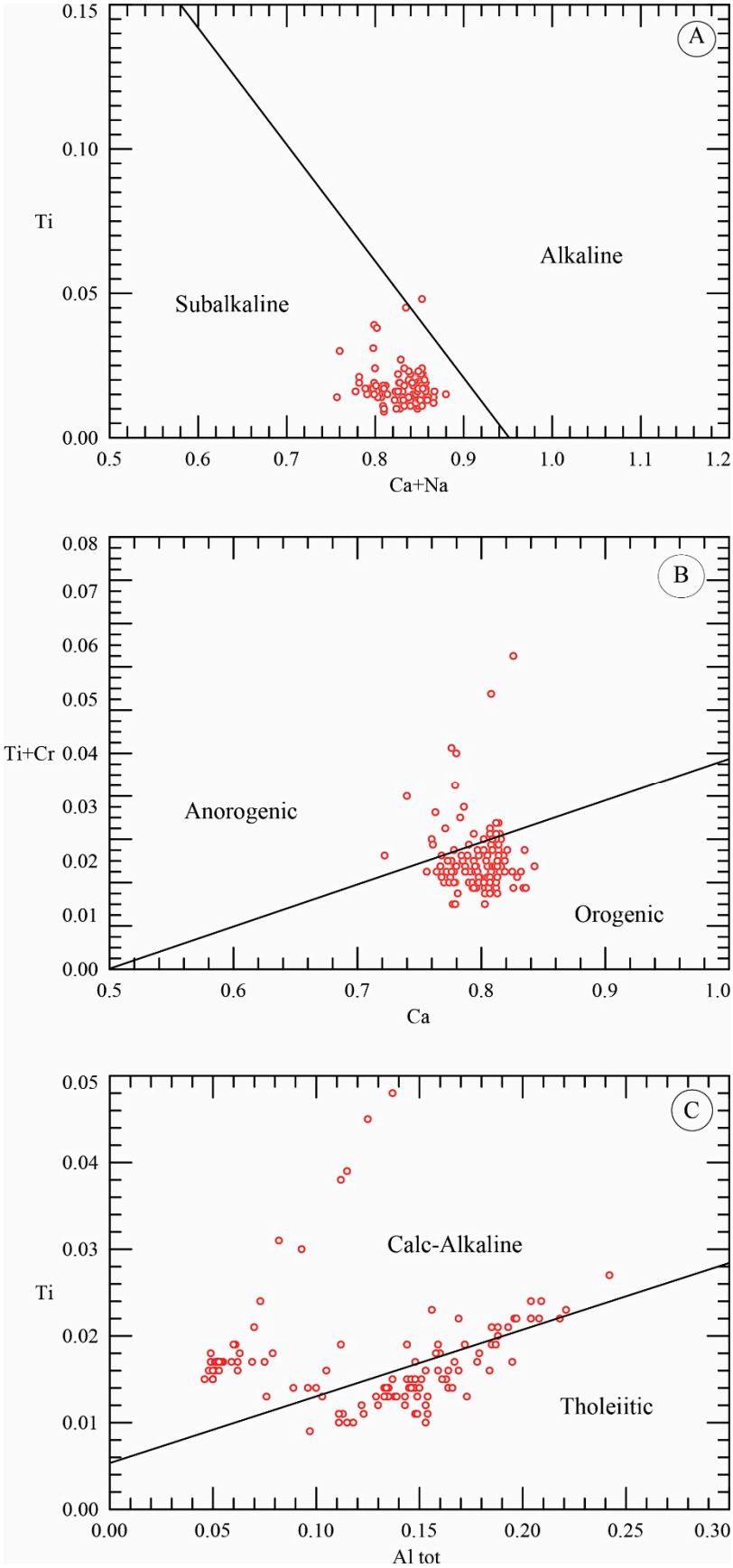

Figure 15. Distribution of the studied clinopyroxenes in three different diagrams: (**A**) Ca + Na–Ti, (**B**) Ca–Ti + Cr, (**C**) Altot–Ti of [63]. Red circles indicate the analyzed clinopyroxenes.

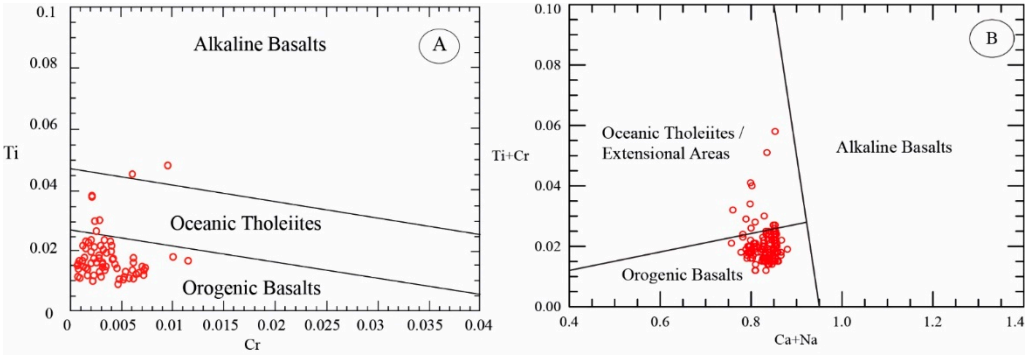

Figure 16. Position of the analyzed clinopyroxenes in the diagrams of [64]: (**A**) Ti–Cr, (**B**) Ti + Cr–Ca + Na. Red circles indicate the analyzed clinopyroxenes.

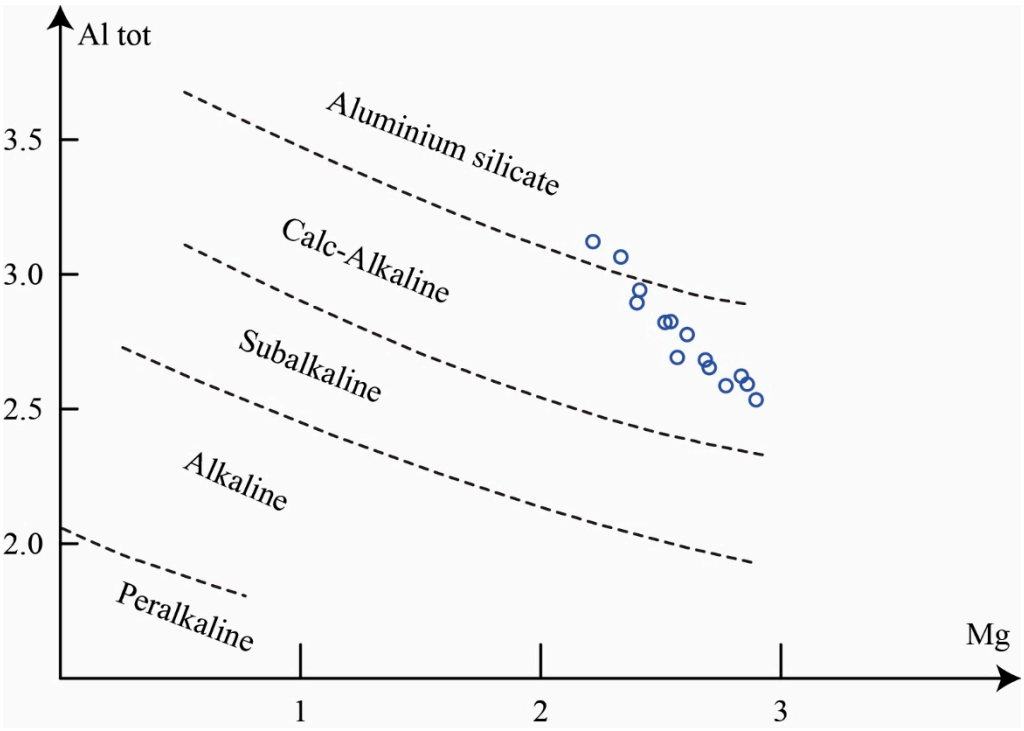

Figure 17. Position of the analyzed biotites in the Altot–Mg diagram of [46]. Blue circles indicate the analyzed Biotites.

5.2. Petrogenesis of TSESDAI Rocks

Calc-alkaline rocks are abundant along destructive plate margins, but calc-alkaline geochemistry is not an indisputable indicator of sin-subduction processes [65]. Indeed calc-alkaline rocks are also known from regions undergoing extension without a time correlated subduction, such as the Basin and Range province [66], the Mexican Volcanic Belt [65], or the northern Da Hinggan Mountains in China [67].

The Paleozoic geology of Morocco was shaped by the Variscan orogeny, with continental collision, between 360 and 290 Ma, having occurred at circa 330–300 Ma, i.e., some 44–14 or even 4 Ma before the emplacement of the studied rocks. This indicates that the generation of the magmas at the origin of the studied rocks cannot be associated with an operating subduction process [25].

When compared to some reference calc-alkaline volcanic series (e.g., calc-alkaline basalts of island arcs [68]; calc-alkaline andesites and dacites of active margins [69]; calc-alkaline andesites of the Tertiary volcanic province of the Basin and Range in the western USA [70]), the chemical composition means and element ratios of andesites and dacites of the TSESDAI volcanics demonstrate that they display greater similarities with the calc-

alkaline series not linked to active subduction, being more similar to those generated in intracontinental extensional settings, as is the case of the Tertiary volcanic province of the Basin and Range (e.g., [71]). However, the Permian andesites of Tiddas is enriched in TiO_2, P_2O_5, Rb, and Cr and depleted in SiO_2, MnO, Sr, Ba, Nb, Hf, and Y. On the other hand, the elemental ratios of the Moroccan Permian andesites and those of the Basin and Range are usually very similar and thus confirm the intraplate calc-alkaline character of the volcanic rocks studied in the present paper. On a first approach, these comparative results suggest that the studied rocks have the same genetic origin as the lavas of the Basin and Range, i.e., petrogenesis involving both fractional crystallization and crustal contamination processes [70].

5.2.1. Fractional Crystallization

Based on their petrographic and geochemical data/criteria, the least differentiated terms of the volcanic materials (the andesites) do not represent primary liquids which have been in equilibrium with the residual paragenesis resulting from partial melting of the common mantle sources. Indeed, they are characterized by low Mg# (0.816 to 0.961) and concentrations in the incompatible element Ni (41 to 58). The POAM (plagioclase–olivine/orthopyroxene–augite–magnetite) crystal fractionation model is a widely accepted process to explain the genesis of andesitic magmas from primary mantle liquids of basaltic composition, and by extension, the mode of evolution of calc-alkaline magmas [72]. The sub-parallel normalized trace elements distribution, as well as the behavior of major and trace elements as a function of silica and Th used as differentiation indices and the decrease of transition elements during the magma evolution clearly show the role played by fractional crystallization in the petrogenesis of the andesites–dacites–rhyolites series of the TSESDAI basin

5.2.2. Crustal Contamination

The existence of enclaves in the lavas of the TSESDAI massif led to the assumption of a magmatic evolution partially controlled by crustal contamination mechanisms. The participation of such processes is also suggested by two observations: (i) the abnormally high contents of Rb, Ba, Th, and La; and (ii) the systematic anomalies in TiO_2 and P_2O_5. The intervention of the continental crust in the petrogenesis could also explain the following facts:

(i) The absence of basalts and the low volume of andesites compared to dacites and rhyolites. According to [72,73], a thick continental crust would have the effect of prolonging the ascent of basaltic and andesitic flows, and thus the fractional crystallization of minerals at low pressure, therefore favoring differentiation and assimilation until reaching the ultimate rhyodacitic to rhyolitic terms;

(ii) The specific chemical characteristics of the andesites such as the enrichment in highly incompatible elements (Rb, Ba, Th, Sr, K_2O, and La) and high ratios (La/Th = 2, 93 to 3; 2.97 on average).

It is interesting to note that Ti and Nb negative anomalies increase with the increasing degree of magmatic evolution, which argues in favor of the conjunction of assimilation and fractional crystallization processes (the ACF process of [74]), a consequence of the exothermic behavior of crystallization processes. The fact that even the least fractionated rocks (the andesites) present such Nb and Ti anomalies suggests that the source of magmas could have some supra-subduction fingerprints inherited from previous subduction events, most probably the Variscan subduction that occurred some 420–330 Ma before [25].

5.3. Volcanological History and Formation Model of the TSESDAI Rocks

The geological and paleogeographical context of the TSESDAI region during the Permian period (deposits within intramontanous continental half-grabens) and the low volume of the outcropping materials (24 km^3) are indicative of an intraplate continental environment. In addition, the lava flows show features suggesting aerial-type eruption

for the TSESDAI volcanism such as the absence of pillow lavas and the presence of flows breccias. Indeed, the pyroclastic formations have juvenile pyroclastic fragments with extensive vesiculation and accreted lapilli. These characteristics are generally ascribed to aerial to sub-aerial environments. Intra-volcanic epiclastites have features of continental fluvial sedimentary rocks. The volcanism of the TSESDAI basin is bimodal, and it is characterized by a predominance of rhyolitic and andesitic facies over dacitic ones. The emissions of andesitic and dacitic magmas take place mainly in the form of lava flows of limited extent, whereas the rhyolitic facies occur in the form of dikes, domes, and pyroclastic fall deposits (deposits of aerial fallout). The volcanological history of the TSESDAI complex is relatively simple when compared to other Moroccan complexes (e.g., Khenifra). It includes three well constrained episodes. The first episode is found in the southwestern boundary (columns A and B, Figure 4) and in the northeastern zone (column E, Figure 4). The volcanic activity begins with the emplacement of pyroxene-rich andesitic flows ("Tiddas andesites"), followed by weak deposits of lapilli, lapilli tuff, and andesitic ashes with volcanological characteristics similar to typical volcanic aerial fallout deposits. Far from the emission centers (characterized by relatively powerful accumulations (50m) and facies diversities; Glimis sector) (F1), a fluvial sedimentation is established including conglomerates with basal pebbles and andesites (alluvial fan deposits) and fallout of aerial projections of andesitic characteristics (andesites to the SW and rhyolites to the NE). The thickness of the andesitic units is between 15 and 40 m, and the total pile reaches nearly 50 m. Contemporaneously with the emplacement of the Tiddas andesitic flows, a dome-like structure is established at the northwestern limit of the volcanic complex (column E, Figure 4), followed by the emplacement of rhyolitic dikes. These domes might be classified as "dome-pistachios", "dome-pistons", or "plug domes" according to the classification of [75]. The second episode, recorded in the central part of the basin (columns C and D, Figure 4) consists of dacite and andesite flows with olivine and pyroxene. The only witnesses of the latter episode are the Bled Bou Haouza and Tabahart outcrops. The last episode was recorded only in the southeastern part of the complex, NE of Tiddas (Figure 2). It is characterized by the emplacement of NE–SW-oriented pyroxene/dolerite dikes. The basaltic flows of El Gitoune (50 m) probably constitute the effusive witnesses of this episode. This episode would be equivalent to the pyroxene dolerites of Khenifra. The vent system is distributed over the entire volcanic domain and is generally oriented parallel to the NE–SW direction of the structures and fractures. Even if this volcanism is basically decentralized, a restricted area (Ari Al Mahsar Sector, southeast of Sebt Ait ikko) has a relatively high density of dikes and domes with high petrographic diversities, i.e., a volcanic apparatus. Based on all the characteristics previously described, the volcanism of the TSESDAI basin can be ascribed to a continental strato-volcano model. However, as in Khenifra, the absence of associated pyroclastic flows (ignimbrites) and pyroclastite deposits in the TSESDAI region is a peculiarity that differentiates the Permian volcanism of western Morocco from the Viseo–Namurian volcanism of eastern Morocco, where caldera-type structures associated with the emission of important ignimbritic layers are notorious [76–79].

5.4. Links between Volcanism and Tectonics in the TSESDAI Basin

The Tiddas-Souk Es Sebt region was subjected during the Permian to an essentially compressive regime [29,80,81], with four deformation episodes, the first three mainly compressive and the fourth corresponding to an extensional event. Among the compressional episodes, the first one is transpressional, with a N50 to N60 compressional direction. This episode is responsible for the opening of the TSESDAI Permian basin following left-lateral N60–N90 strike-slip accidents and the extrusion of the first andesitic and rhyolitic volcanism. A N10–N40 to N70 syn-sedimentary normal-fault system can be clearly associated with this episode. This fault system guides the collapse of the blocks and thus lead to the individualization of Permian grabens and half-grabens. The NW–SE extension, developed by this transtensional regime and guided by the rework of normal faults inherited from the Hercynian major phases, gave rise to a series of collapsed blocks. Thus, the Permian

graben and half-graben structures clearly resulted from this phase. The opening of deep extensional fractures in the Paleozoic substratum allowed the extrusion of the first volcanic series (the rhyolitic domes and associated rhyolitic dikes to the northeast and the Tiddas andesitic flows) and conditioned the Permian sedimentation. The second episode is a WNW–ESE-oriented compressional regime. It triggered conjugate strike-slip fault systems affecting the Permian deposits: N80 to N90 right-lateral faults and N140–150 left-lateral faults. The later fault system transected the normal faults triggered during the first tectonic event (NW–SE extension). The third tectonic episode involved NNW–SSE to N–S regional compression, reactivating some N40–N70 normal faults into inverse ones. This episode is also responsible for the N80-oriented-axis of the large-radius folds deforming the Permian detrital deposits. The fourth episode is a NW–SE extensional event accompanied by N40 to N60 normal faults that gave rise to a series of collapsed blocks. The age of this extensional episode remains unknown. However, the fact that the faults generated during this episode affect only the basal conglomerates of the Triassic series and that its extension direction is compatible with the dolerite dikes of the El Gnoune sector suggest a Late Permian to Early/Middle Triassic age. On the map of Figure 18, we represented different characteristics of the emission centers (cumulo-domes, sills, maximum thicknesses of flows, and the diversity of eruptive mechanisms) and the major accidents that acted as rifts during the Permian. We suggest that the dikes and the emission points are mostly aligned along N40–N70 accidents whose complex and polyphase play triggered the chaotic peeling off characteristics of the deformation. The magma emission would occur by injection, either in relays of major accidents, or as en echelon tension cracks or normal faults. The direction of shortening Z or compression σ1 can be deduced from the direction of the dikes: N50 to N90 with a clear predominance of the N60 direction, which coincides with the alignment of the emission centers. This direction is similar to the N50–60 compressional vector that controlled the opening of the basin: relay-basins along left-lateral accidents. It should also be noted that the inclination of the veins is compatible with the strike-slip movement along these accidents.

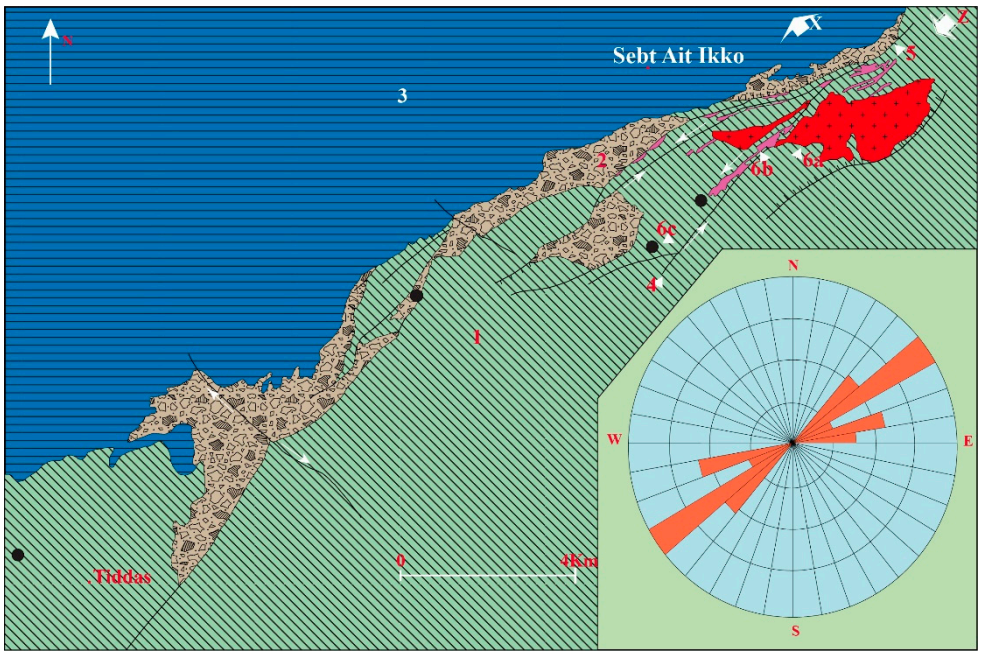

Figure 18. Structural control of emission centers in the Permian volcanics of the TSESDAI volcanic complex: (1) Pre-Permian Paleozoic basement; (2) Autunian conglomerates, sandstones, and mudstones; (3) Mesozoic and Tertiary formations; (4) left-lateral fault; (5) normal faults; (6) emission centers, domes (6a), veins (6b), and maximum thickness of flows (6c). Z, direction of shortening; X, direction of extension. The inlet displays a rosette of the directions and cumulative lengths of the rhyolitic veins.

5.5. Geochronological Constraints

The SHRIMP U–Pb geochronologic data of zircons recovered from the rhyolite dome of Ari El Mahsar in the TSESDAI basin shows a Concordia age of 286.4 ± 4.7 Ma (MSWD of concordance = 0.47, probability of concordance = 0.49) interpreted to date the magmatic crystallization of this dome (Figure 14, Table 2). According to the stratigraphic framework of [6,27], this age should be older than the andesites of the first pulse and the dacites of the second one [23]. The 286.4 ± 4.7 Ma dating agrees with an Artinskian–Kungurian age attributed to the clastic succession in relation with their flora and macrofauna (e.g, ichnofauna) content of [23,33,34,82]. At the Bou Achouch basin, the C–P sedimentary series is considered by [34] as Kungurian in age based on macroflora assemblages found in their fine-grained clastic units and reworked ash deposits. In addition, similarities between the flora of Bou Achouch and the Lower Rotliegend of the Saar-Nahe Basin (Germany; [83]) extend their age back into the latest Carboniferous. Recently, authors in [23] obtained a weighted mean $^{206}Pb/^{238}U$ age of 301.50 ± 1.24 Ma for an andesite (Table S4). This age is considered the best estimate of the eruption moment of the andesite. According to [23], the flora studied by [34] are indeed older than Kungurian (~283–273 Ma), similar to what occurs with the flora of the Lower Rotliegened (latest Carboniferous to early Permian) sediments of the Saar-Nahe Basin in Germany [83], considering that this andesite represents indeed the top of the stratigraphic sequence at Bou Achouch as suggested by the stratigraphic analyses of [6]. However, according to [23], the latter stratigraphic framework is composite, as the basin stratigraphy is disturbed by thrusts. Therefore, the possibility that some andesites stratigraphically lie below the fossil-bearing units cannot be excluded. Previous ages of the volcanic rocks of the Khenifra basin comprise a K–Ar whole rock age of 264 ± 10 Ma obtained from a rhyolitic breccia at Jbel Bou Hayati [84]. At the same locality, the volcanic pile that was assigned to the early Permian contains fossil wood [34,85,86]. Recently LA–ICP–MS U–Pb (on zircon) ages from several volcanic localities in Khenifra were published by [87], including a dacite from the lower lava flows at Jbel Taghat (295.1 ± 2.9 Ma) and interpreted as the oldest volcanic pulse of Khenifra. The dome of Sidi Tir delivered ages ranging from 290.3 ± 2.1 Ma to 287.9 ± 3.8 Ma, thus suggesting that the dome was emplaced during ~2 Ma. Rhyolitic pyroclastic fall deposits from Sidi Tir yielded two predominant age clusters at 307.3 ± 2.6 Ma and 290.6 ± 2.6 Ma. The latter age was thought to be more concordant with the age of the eruption. At Talat Mechtal, inferred to post-date Cisuralian sedimentation in Khenifra, authors in [87] obtained an age of 280.3 ± 2.1 Ma for the upper dacitic lavas, supposedly marking the last volcanic pulse in agreement with the lithostratigraphic sequence [7]. From the same locality, authors in [23] reported a $^{206}Pb/^{238}U$ weighted mean-age of 305.59 ± 2.68 Ma for an andesite lava laying at the base of the Talat Mechtal volcanic succession, overlain by 290.6 ± 2.6 Ma pyroclastic fall deposits [87]; this implies that volcanism at Talat Mechtal began ~15 Ma earlier than previously thought [87]. In the Chougrane and Souk el Had Bouhsoussène basins, the age of the sedimentary package is not well constrained; on the basis of its similarity with the facies of the Khenifra and TSESDAI basins it is assumed that the date might be early Permian. The sedimentary package is overlain by the Bir el Gassaa andesites dated to 270 ± 17 Ma by whole rock K–Ar techniques [88]. Two samples, an andesite from Bir el Gassaa that lies on the top of the C–P stratigraphic sequence of Chougrane and an andesite from Souk el Had Bouhsoussène, were recently dated by [23]. The first sample only provided three concordant ages that range from 307.8 ± 4 to 295.5 ± 3.4 Ma, implying that the underlying C–P sediments are earliest Permian or late Carboniferous [23]. The andesitic sample from Souk el Had Bouhsoussène sub-basin has $^{206}Pb/^{238}U$ ages ranging between 295.6 ± 2.9 and 267.9 ± 3.9 Ma. According to existing stratigraphic models of the Chougrane CPB, the andesitic sample from Bir el Gassaa is considered to lie stratigraphically above the andesitic sample from Souk el Had Bouhsoussène sub-basin and is thus expected to be younger. According to [23], the existing stratigraphic model would require consideration as the crystallization age of the youngest value of 295.5 ± 3.4 Ma and 295.6 ± 2.9 Ma from the two dated samples. Even if these geochronological results are clearly inadequate to obtain

solid conclusions, they provisionally suggest that the Souk el Had Bouhsoussène sub-basin is younger than the Chougrane one, and therefore the two basins evolved independently, in contrast to the above-mentioned stratigraphic models. The youngest age of the andesitic sample from Souk el Had Bouhsoussène sub-basin could offer a valid constraint on the final phase of the Variscan tectonism, since this basin was tilted during this stage [23]. In the Mechra Ben Abbou basin of "Bled Mekrach", authors in [89] obtained a 611 ± 20 Ma U–Pb SHRIMP age on zircon from a rhyolitic dome, supposedly inherited from zircons of the Pan-African basement of the Rehamna massif and a younger more concordant age of 285.3 ± 4.9 Ma interpreted as the age of crystallization of the rhyolitic dome [89]. South of the basin, a microgranitic/microdioritic dike swarm intruding the pre-Permian basement has been dated to 285.4 ± 6.1 Ma (U–Pb on zircon) [89–92]. Two samples, from an andesite flow and an andesite plug (Douar Ouled Said Ben Ali lavas), provided concordant $^{206}Pb/^{238}U$ (on zircon) ages of 284.2 ± 4.6 and 294.63 ± 0.67 Ma, respectively. The younger age of 284.2 ± 4.6 Ma would imply that volcanism could have begun in this basin at least 10 Ma earlier [23]. In the Nzalet el Hararcha basin, sediments are sealed by Permian lavas dominated by andesites and calc-alkaline rhyolitic domes [38,89,93–95], and the entire basinal sequence is unconformably covered by Cretaceous and Cenozoic rocks [95]. A rhyolitic sample (Sidi Bou Yahia dome) provided a robust $^{206}Pb/^{238}U$ weighted mean age of 277.07 ± 0.61 Ma, which represents the first absolute age constraint from this basin [23].

6. Conclusions

The main conclusions of this study are summarized below:

(1) The volcanic characteristics of the TSESDAI volcanic complex and the distribution of the emission centers and their structural control suggest a multi-vent continental stratovolcano-type facies model.

(2) The Ari Al Mahssar area has a relatively high density of dikes and domes and a remarkable petrographic diversity indicative of a possible volcanic apparatus.

(3) The mineralogy of the primary crystals (biotite and clinopyroxenes) and the morphological typology of the zircons of the TSESDAI volcanic rocks suggest a calc-alkaline orogenic magmatic setting.

(4) The geochemical study of major and trace elements confirms the intracontinental calc-alkaline signature of the studied rocks, similar to the andesites of the American Basin and Range extensional realm.

(5) The geochemical study also indicates an evolution controlled by fractional crystallization and crustal contamination (assimilation).

(6) The petrographic and volcanological characteristics of the TSESDAI volcanic series (in particular the first and the second episodes) suggest a similarity with the well-defined first Permian cycle of the Khenifra region, with the exception of the dolerite dikes and the basaltic flows of El Gitoune (third episode) that belong to the second Permian cycle, despite their similar NE–SW alignment to the first and the second episodes studied here.

(7) The TSESDAI basin recorded four Permian deformation episodes. The first one is responsible for the opening of the Permian basin along N60–N90 left-lateral strike-slip accidents and the establishment of the first andesitic and rhyolitic volcanic episode. The second one is defined by a conjugated system of faults affecting the Permian deposits. The third compressive episode (NNW–SSE to N–S orientation of σ1) reactivates some N40–N70 normal faults into inverse faults. The fourth episode is a NW–SE trending extensional event triggering N40 to N60 normal faults and consequent collapsed blocks.

(8) The SHRIMP U–Pb geochronologic data of zircons recovered from the rhyolitic dome of Ari El Mahsar in the TSESDAI basin show a Concordia age of 286.4 ± 4.7 Ma interpreted to date the magmatic crystallization of this dome. Thus, this rhyolite belongs likely to the third magmatic episode of the region.

Supplementary Materials: The following are available online at https://www.mdpi.com/article/10.3390/min11101099/s1, Table S1: Chemical analysis of dacite clinopyroxenes from Tiddas-Souk Es Sebt des Ait Ikko volcanic complex, and their structural formula calculated on the basis of 6 oxygens, Table S2: Chemical analysis of dacites orthopyroxenes from Tiddas-Souk Es Sebt des Ait Ikko volcanic complex, and their structural formula calculated on the basis of 6 oxygens, Table S3: Chemical analysis of rhyolite biotites in dome of Tiddas-Souk Es Sebt des Ait Ikko volcanic complex and their structural formulas calculated on the basis of 22 oxygens, Table S4: Overview of new and published geochronological data from Carboniferous–Early Permian basins of central Morocco (after [23]).

Author Contributions: Conceptualization, I.H., N.Y., and A.A.L.; methodology, N.Y.; software, I.H., A.A.L., O.M., and W.E.M.; validation, N.Y., J.M., and M.D.; formal analysis, C.C.G.T., M.A.S.B., and K.S; investigation, I.H., N.Y., and A.A.L.; resources, N.Y.; data curation, N.Y., A.A.L., and W.E.M.; writing—original draft preparation, I.H., N.Y., and A.A.L.; writing—review and editing, O.M., J.M., M.D., L.G., M.A.S.B., K.S., W.E.M., and M.A.B.; visualization, I.H.; supervision, N.Y., M.K.B., and M.A.B.; project administration, N.Y., M.K.B., and M.A.B.; funding acquisition, C.C.G.T. All authors have read and agreed to the published version of the manuscript.

Funding: This work was funded by the Universidade de São Paulo: USP-UCAM/2016, the Russian Science Foundation: Mega-Grant 14.Y26.31.0012, and by the FCT—Fundação para a Ciência e a Tecnologia: UIDB/50019/2020.

Data Availability Statement: Not Applicable.

Acknowledgments: Most of this work was carried out at the Department of Geology of the Faculty of Sciences-Semlalia, Cadi Ayyad University of Marrakech and the "Centro de Pesquisas Geocronológicas (CPGeo), Instituto de Geociências (IG), Universidade de São Paulo-USP, São Paulo (SP), Brazil" within the framework of the scientific and technical agreement between the São Paulo University and the Cadi Ayyad University (responsibles Colombo Celso Gaeta Tassinari and Nasrrddine Youbi). João Mata acknowledges the financial FCT support through project UIDB/50019/2020-IDL. Nasrrddine Youbi is supported by Russian Mega-Grant 14.Y26.31.0012.

Conflicts of Interest: The authors declare no conflict of interest.

References

1. Doblas, M.; Oyarzun, R.; López-Ruiz, J.; Cebriá, J.M.; Youbi, N.; Mahecha, V.; Lago, M.; Pocoví, A.; Cabanis, B. Permo-Carboniferous volcanism in Europe and northwest Africa: A superplume exhaust valve in the centre of Pangaea? *J. Afr. Earth Sci.* **1998**, *26*, 89–99. [CrossRef]
2. Wilson, M.; Neumann, E.R.; Davies, G.R.; Timmerman, M.J.; Heeremans, M.; Larsen, B.T. Permo-carboniferous magmatism and rifting in Europe: Introduction. *Geol. Soc. Spec. Publ.* **2004**, *223*, 1–10. [CrossRef]
3. Youbi, N.; Ernst, R.E.; Mitchell, R.N.; Boumehdi, M.A.; El Moume, W.; Lahna, A.A.; Bensalah, M.K.; Söderlund, U.; Doblas, M.; Tassinari, C.C.G. Preliminary Appraisal of a Correlation Between Glaciations and Large Igneous Provinces Over the Past 720 Million Years. In *Large Igneous Provinces: A Driver of Global Environmental and Biotic Changes*; John Wiley & Sons: Hoboken, NJ, USA, 2021; pp. 169–190. [CrossRef]
4. Arthaud, F.; Matte, P. Les decrochements tardi-hercyniens du sud-ouest de l'europe. Geometrie et essai de reconstitution des conditions de la deformation. *Tectonophysics* **1975**, *25*, 139–171. [CrossRef]
5. Arthaud, F.; Matte, P. Late Paleozoic strike-slip faulting in southern Europe and northern Africa: Result of a right-lateral shear zone between the Appalachians and the Urals. *Bull. Geol. Soc. Am.* **1977**, *88*, 1305–1320. [CrossRef]
6. Cailleux, Y.; Gonord, H.; Le guern, M.; Sauvage, M. Taphrogenèse et magmatisme permien dans le Maroc Central. *Bull. Fac. Sci. Marrakech.* **1983**, *1*, 24–39.
7. Youbi, N.; Cabanis, B.; Chalot-Prat, F.; Cailleux, Y. Histoire volcano-tectonique du massif permien de Khénifra (Sud-Est du Maroc central). *Geodin. Acta* **1995**, *8*, 158–172. [CrossRef]
8. Van Hilten, D. Evaluation of some geotectonic hypotheses by paleomagnetism. *Tectonophysics* **1964**, *1*, 3–71. [CrossRef]
9. Elter, F.M.; Gaggero, L.; Mantovani, F.; Pandeli, E.; Costamagna, L.G. The Atlas-East Variscan -Elbe shear system and its role in the formation of the pull-apart Late Palaeozoic basins. *Int. J. Earth Sci.* **2020**, *109*, 739–760. [CrossRef]
10. Timmerman, M.J.; Heeremans, M.; Kirstein, L.A.; Larsen, B.T.; Spencer-Dunworth, E.A.; Sundvoll, B. Linking changes in tectonic style with magmatism in northern Europe during the late Carboniferous to latest Permian. *Tectonophysics* **2009**, *473*, 375–390. [CrossRef]
11. Upton, B.G.J.; Stephenson, D.; Smedley, P.M.; Wallis, S.M.; Fitton, J.G. Carboniferous and Permian magmatism in Scotland. *Geol. Soc. Spec. Publ.* **2004**, *223*, 195–218. [CrossRef]

12. Ernst, R.E.; Buchan, K.L. Layered mafic intrusions: A model for their feeder systems and relationship with giant dyke swarms and mantle plume centres. *S. Afr. J. Geol.* **1997**, *100*, 319–334.
13. Torsvik, T.H.; Steinberger, B.; Cocks, L.R.M.; Burke, K. Longitude: Linking Earth's ancient surface to its deep interior. *Earth Planet. Sci. Lett.* **2008**, *276*, 273–282. [CrossRef]
14. Kirstein, L.A.; Dunai, T.J.; Davies, G.R.; Upton, B.G.J.; Nikogosian, I.K. Helium isotope signature of lithospheric mantle xenoliths from the Permo-Carboniferous magmatic province in Scotland—No evidence for a lower-mantle plume. *Geol. Soc. Spec. Publ.* **2004**, *223*, 243–258. [CrossRef]
15. Veevers, J.J.; Powell, C.M. Late Paleozoic glacial episodes in Gondwanaland reflected in transgressive- regressive depositional sequences in Euramerica. *Geol. Soc. Am. Bull.* **1987**, *98*, 475–487. [CrossRef]
16. Crowell, J.C. *Pre-Mesozoic Ice Ages: Their Bearing on Understanding the Climate System*; Geological Society of America, Inc.: Boulder, CO, USA, 1999; Volume 192, ISBN 0813711924.
17. Isbell, J.L.; Miller, M.F.; Wolfe, K.L.; Lenaker, P.A. *Timing of Late Paleozoic Glaciation in Gondwana: Was Glaciation Responsible for the Development of Northern Hemisphere Cyclothems?* Special Paper of The Geological Society of America; Geological Society of America, Inc.: Boulder, CO, USA, 2003; Volume 370. [CrossRef]
18. Cather, S.M.; Dunbar, N.W.; McDowell, F.W.; McIntosh, W.C.; Scholle, P.A. Climate forcing by iron fertilization from repeated ignimbrite eruptions: The icehouse-silicic large igneous province (SLIP) hypothesis. *Geosphere* **2009**, *5*, 315–324. [CrossRef]
19. El Wartiti, M.; Broutin, J.; Freytet, P.; Larhrib, M.; Toutin-Morin, N. Continental deposits in Permian basins of the Mesetian Morocco, geodynamic history. *J. Afr. Earth Sci.* **1990**, *10*, 361–368. [CrossRef]
20. Saber, H.; El-Wartiti, M.; Broutin, J.; Toutin Morin, N. L'intervalle stephano-permien (fin du cycle varisque au Maroc). *Gaia* **1995**, *11*, 57–71.
21. Saber, H.; El Wartiti, M. Histoire sédimentaire et tectonique tardi-hercynienne des bassins de l'Oued Zat et Ida Ou Zal (Haut Atlas occidental, Maroc): Bassins en transtension sur décrochements. *J. Afr. Earth Sci.* **1996**, *22*, 301–309. [CrossRef]
22. Abbou, M.B.; Soula, J.C.; Brusset, S.; Roddaz, M.; N'Tarmouchant, A.; Driouch, Y.; Christophoul, F.; Bouadbelli, M.; Majesté-Menjoulas, C.; Béziat, D.; et al. Contrôle tectonique de la sédimentation dans le système de bassins d'avant-pays de la Meseta marocaine. *C. R. Acad. Sci. Ser. IIA Earth Planet. Sci.* **2001**, *5*, 703–709. [CrossRef]
23. Domeier, M.; Font, E.; Youbi, N.; Davies, J.; Nemkin, S.; Van der Voo, R.; Perrot, M.; Benabbou, M.; Boumehdi, M.A.; Torsvik, T.H. On the Early Permian shape of Pangea from paleomagnetism at its core. *Gondwana Res.* **2021**, *90*, 171–198. [CrossRef]
24. Hoepffner, C.; Soulaimani, A.; Piqué, A. The Moroccan Hercynides. *J. Afr. Earth Sci.* **2005**, *43*, 144–165. [CrossRef]
25. Michard, A.; Soulaimani, A.; Hoepffner, C.; Ouanaimi, H.; Baidder, L.; Rjimati, E.C.; Saddiqi, O. Tectonophysics The South-Western Branch of the Variscan Belt: Evidence from Morocco. *Tectonophysics* **2010**, *492*, 1–24. [CrossRef]
26. Michard, A.; Ouanaimi, H.; Hoepffner, C.; Soulaimani, A.; Baidder, L. Comment on Tectonic relationships of Southwest Iberia with the allochthons of Northwest Iberia and the Moroccan Variscides by J.F. Simancas et al. [C. R. Geoscience 341 (2009) 103–113]. *C. R. Geosci.* **2010**, *342*, 170–174. [CrossRef]
27. Gonord, H.; Le Guern, M.; Turiot, D.; Rebourd, H. Mise en évidence d'un volcanisme rhyolitique stéphano-permien sur la bordure nord du massif hercynien central du Maroc extension et importance du volcanisme tardy-hercynien. *C. R. Acad. Sci.* **1980**, *291*, 51–54.
28. El Wartiti, M. Les Terrains Permo-Carbonifères et Leur Couverture dans la Zone de Tiddas-Souk es Sebt (Bordure Nord-Ouest de la Méséta Marocaine. Nord du Maroc Central). Ph.D. Thesis, Mohamed V, Rabat, Morocco, 1981.
29. Zouine, E.M. Evolution structurale tardi-hercynienne de la bordure septentrionale du Maroc Central entre Tiddas et Jbel Triona. Ph.D. Thesis, E.N.S. Souissi, Rabat, Morocco, 1986.
30. Larhrib, M. Les Formations Permiennes et Triasico-Mio-Quaternaires des Régions de Tiddas, Maaziz et Sebt Aït Ikko (NW du Maroc Central). Stratigraphie, Sédimentologie et Reconstitution des Paléoenvironnements Sédimentaires. Ph.D. Thesis, Ecole Normale Supérieure, Rabat, Morocco, 1988.
31. Larhrib, M. Les formations fluviatiles rouges violacées du bassin permien (Autunien inférieur) de Tiddas-Sebt Aït Ikkou (NW du Maroc Central). In Proceedings of the 8ème Colloque Bassins Sédimentaires, El Jadida, Morocco, 23–25 May 1990; pp. 3–4.
32. Larhrib, M. Flore fossile et séquences des formations rouges fluviatiles du bassin autunien de Tiddas-Sebt Aït Ikkou (nord-ouest du Maroc central). In *Le Permien et le Trias du Maroc: État des Connaissances*; Medina, F., Ed.; Presses Universitaires du Maghreb: Marrakech, Morocco, 1996; pp. 19–29.
33. Voigt, S.; Lagnaoui, A.; Hminna, A.; Saber, H.; Schneider, J.W. Revisional notes on the Permian tetrapod ichnofauna from the Tiddas Basin, central Morocco. *Palaeogeogr. Palaeoclimatol. Palaeoecol.* **2011**, *302*, 474–483. [CrossRef]
34. Broutin, J.; Aassoumi, H.; El Wartiti, M.; Freytet, P.; Kerp, H.; Quesada, C.; Toutin-morin, N. The Permian basins of Tiddas, Bou Achouch and Khenifra (central Morocco). Biostratigraphic and palaeophytogeographic implications. *Mémoires Muséum Natl. d'Histoire Nat.* **1998**, *179*, 257–278.
35. Marchetti, L.; Ronchi, A.; Santi, G.; Schirolli, P.; Conti, M.A. Revision of a classic site for Permian tetrapod ichnology (Collio Formation, Trompia and Caffaro valleys, N. Italy), new evidences for the radiation of captorhinomorph footprints. *Palaeogeogr. Palaeoclimatol. Palaeoecol.* **2015**, *433*, 140–155. [CrossRef]
36. Termier, H. Etudes géologiques sur le Maroc Central et le Moyen Atlas septentrional, Rabat. 1936. Available online: https://www.persee.fr/doc/rga_0035-1121_1937_num_25_3_3982_t1_0525_0000_1 (accessed on 20 May 2021).

37. Michard, A. *Elements de Geologie Marocaine*; Notes et Memoires du Service Geologique No. 252; Editions du Service Geologique du Maroc: Rabat, Morroco, 1976; p. 408.
38. Youbi, N. Le Volcanisme "Post-Collisionnel" un Magmatisme Intraplaque Relié à des Panaches Mantelliques. Etude Volcanologique et Géochimique. Exemple d'application dans le Néoprotérozoique Terminal (PIII) de l'Anti-Atlas et le Permien du Maroc. Ph.D. Thesis, Faculty SEMLALIA, CAdi AYYAD, Marrakesh, Morocco, 1998.
39. Black, L.P.; Kamo, S.L.; Allen, C.M.; Davis, D.W.; Aleinikoff, J.N.; Valley, J.W.; Mundil, R.; Campbell, I.H.; Korsch, R.J.; Williams, I.S.; et al. Improved 206Pb/238U microprobe geochronology by the monitoring of a trace-element-related matrix effect; SHRIMP, ID-TIMS, ELA-ICP-MS and oxygen isotope documentation for a series of zircon standards. *Chem. Geol.* **2004**, *205*, 115–140. [CrossRef]
40. Williams, I.S. U-Th-Pb geochronology by ion microprobe. In *Applications of Microanalytical Techniques to Understanding Mineralising Processes*; McKibben, M., Shanks, W., Riley, W., Eds.; Reviews in Economic Geology; Society of Economic Geologists: Littleton, CO, USA, 1998; pp. 1–35.
41. Ludwig, K.R. Isoplot 3: A Geochronological Toolkit for Microsoft Excel. *Berkeley Geochronol. Cent.* **2003**, *4*, 70.
42. Ouabid, M.; Garrido, C.J.; Ouali, H.; Harvey, J.; Hidas, K.; Marchesi, C.; Acosta-Vigil, A.; Dautria, J.M.; El Messbahi, H.; Román-Alpiste, M.J. Late Cadomian rifting of the NW Gondwana margin and the reworking of Precambrian crust–evidence from bimodal magmatism in the early Paleozoic Moroccan Meseta. *Int. Geol. Rev.* **2020**, 1–24. [CrossRef]
43. Morimoto, N. Nomenclature of Pyroxenes. *Mineral. Petrol.* **1988**, *39*, 55–76. [CrossRef]
44. Tiba, T. Titaniferous Biotites and Associated Phenocrysts in Dike Rocks From Dozen, Oki Islands. *J. Jpn. Assoc. Mineral. Petrol. Econ. Geol.* **1972**, *67*, 357–369. [CrossRef]
45. Le Bel, L. Micas magmatiques et hydrothermaux dans l'environnement du porphyre cuprifère de Cerro Verde-Santa Rosa, Pérou. *Bull. Minéral.* **1979**, *102*, 35–41. [CrossRef]
46. Nachit, H.; Razafimahefa, N.; Stussi, J.; Carron, J. Composition chimique des biotites et typologie magmatique des granitoïdes. *C. R. Acad. Sci.* **1985**, *301*, 813–818.
47. Abdel-Rahman, A.F.M. Nature of biotites from alkaline, calc-alkaline, and peraluminous magmas. *J. Petrol.* **1994**, *35*, 525–541. [CrossRef]
48. Deer, W.; Howie, R.A.; Zussman, J. *An Introduction to Rock-Forming Minerals*; Mineralogical Society of Great Britain & Ireland: London, UK, 1966.
49. Bas, M.J.L.; Maitre, R.W.L.; Streckeisen, A.; Zanettin, B. A chemical classification of volcanic rocks based on the total alkali-silica diagram. *J. Petrol.* **1986**, *27*, 745–750. [CrossRef]
50. Miyashiro, A. Nature of alkalic volcanic rock series. *Contrib. Mineral. Petrol.* **1978**, *66*, 91–104. [CrossRef]
51. Harker, A. Igneous rock-series and mixed igneous rocks. *J. Geol.* **1900**, *8*, 389–399. [CrossRef]
52. Saunders, A.; Tarney, J.; Marsh, N.; Wood, D. Ophiolites as oceanic crust or marginal basin crust: A geochemical approach. In Proceedings of the Ophiolites International Ophiolite Symposium, Nicosia, Chyprus, 1–8 April 1979; pp. 193–204.
53. Cabanis, B. Identification des Séries Magmatiques dans les Socles Métamorphiques sur la Base de Critères Géologiques, Pétrographiques et Géochimiques. Ph.D. Thesis, P. et M.-Curie, Paris, France, 1986.
54. Thorpe, R.S.; Leat, P.T.; Mann, A.C.; Howells, M.F.; Reedman, A.J.; Campbell, S.D.G. Magmatic evolution of the ordovician snowdon volcanic centre, North Wales (UK). *J. Petrol.* **1993**, *34*, 711–741. [CrossRef]
55. Harris, N.B.W.; Pearce, J.A.; Tindle, A.G. *Geochemical Characteristics of Collision-Zone Magmatism*; Special Publications; Geological Society: London, UK, 1986; Volume 19, pp. 67–81. [CrossRef]
56. Pupin, J.P. Zircon and granite petrology. *Contrib. Mineral. Petrol.* **1980**, *73*, 207–220. [CrossRef]
57. Hoskin, P.W.O.; Schaltegger, U. The composition of zircon and igneous and metamorphic petrogenesis. *Rev. Mineral. Geochem.* **2003**, *53*, 27–62. [CrossRef]
58. Linnemann, U.; Gerdes, A.; Drost, K.; Buschmann, B. The continuum between Cadomian orogenesis and opening of the Rheic Ocean: Constraints from LA-ICP-MS U-Pb zircon dating and analysis of plate-tectonic setting (Saxo-Thuringian zone, northeastern Bohemian Massif, Germany). *Spec. Pap. Geol. Soc. Am.* **2007**, *423*, 61–96. [CrossRef]
59. Winchester, J.A.; Floyd, P.A. Geochemical discrimination of different magma series and their differentiation products using immobile elements. *Chem. Geol.* **1977**, *20*, 325–343. [CrossRef]
60. Pearce, J.A. Geochemical fingerprinting of oceanic basalts with applications to ophiolite classification and the search for Archean oceanic crust. *Lithos* **2008**, *100*, 14–48. [CrossRef]
61. Miyashiro, A. The troodos ophiolitic complex was probably formed in an island arc. *Earth Planet. Sci. Lett* **1973**, *19*, 218–224. [CrossRef]
62. Miyashiro, A. Volcanic rock series in island arcs and active continental margins. *Am. J. Sci.* **1974**, *274*, 321–355. [CrossRef]
63. Leterrier, J.; Maury, R.C.; Thonon, P.; Girard, D.; Marchal, M. Clinopyroxene composition as a method of identification of the magmatic affinities of paleo-volcanic series. *Earth Planet. Sci. Lett.* **1982**, *59*, 139–154. [CrossRef]
64. Mollard, J.; Maury, R.C.; Leterrier, J.; Bourgois, J. Teneurs en chrome et titane des clinopyroxenes calciques des basaltes; Application à l'identification des affinités magmatiques de roches paléovolcaniques. *C. R. Acad. Sci.* **1983**, *296*, 903–908.
65. Sheth, H.C.; Torres-Alvarado, I.S.; Verma, S.P. What is the "calc-alkaline rock series"? *Int. Geol. Rev.* **2002**, *44*, 686–701. [CrossRef]
66. Hawkesworth, C.; Turner, S.; Gallagher, K.; Hunter, A.; Bradshaw, T.; Rogers, N. Calc-alkaline magmatism, lithospheric thinning and extension in the Basin and Range. *J. Geophys. Res.* **1995**, *100*, 10271–10286. [CrossRef]

67. Fan, W.M.; Guo, F.; Wang, Y.J.; Lin, G. Late Mesozoic calc-alkaline volcanism of post-orogenic extension in the northern Da Hinggan Mountains, northeastern China. *J. Volcanol. Geotherm. Res.* **2003**, *121*, 115–135. [CrossRef]
68. Dupuy, C.; Dostal, J.; Marcelot, G.; Bougault, H.; Joron, J.L.; Treuil, M. Geochemistry of basalts from central and southern New Hebrides arc: Implication for their source rock composition. *Earth Planet. Sci. Lett.* **1982**, *60*, 207–225. [CrossRef]
69. Deruelle, B. Petrology of the plio-quaternary volcanism of the South-Central and Meridional Andes. *J. Volcanol. Geotherm. Res.* **1982**, *14*, 77–124. [CrossRef]
70. Gans, P.B.; Mahood, G.A.; Schermer, E. Synextensional magmatism in the Basin and Range Province; A case study from the eastern Great Basin. *Spec. Pap. Geol. Soc. Am.* **1989**, *233*, 1–53. [CrossRef]
71. Putirka, K.; Platt, B. Basin and Range volcanism as a passive response to extensional tectonics. *Geosphere* **2012**, *8*, 1274–1285. [CrossRef]
72. Gill, J. *Orogenic Andesites and Plate Tectonics*; Springer: Berlin/Heidelberg, Germany, 1981.
73. Coulon, C. Le volcanisme calco-alcalin cénozoïque de Sardaigne (Italie). Pétrographie, géochimie et génèse des laves andésitiques et des ignimbrites. Signification géodynamique. Ph.D. Thesis, AIX-MARSEILLE III, Marseille, France.
74. DePaolo, D.J. Trace element and isotopic effects of combined wallrock assimilation and fractional crystallization. *Earth Planet. Sci. Lett.* **1981**, *53*, 189–202. [CrossRef]
75. Emami, M.H.; Michel, R. Les Volcans Dômeens du Néogène de la Région de Qom (Iran Central). Essai de Classification de l'Activité Volcanique Dômeenne. *Bull. Volcanol.* **1982**, *45*, 317–332. [CrossRef]
76. Kharbouch, F. Pétrographie et Géochimie des Laves Dinantiennes de la Méséta Nord-Occidentale et Orientale Marocaine. Ph.D. Thesis, Louis Pasteur, Strasbourg, France, 1983.
77. Kharbouch, F. Le volcanisme dévono-dinantien du Massif central et de la Meseta orientale. *Bull. Inst. Sci.* **1994**, *18*, 192–200.
78. Chalot-Prat, F. Mise en évidence d'une dépression volcanotectonique associée à d'épais épanchements ignimbritiques hercyniens dans le massif du Tazekka (Maroc oriental). *Rev. Géologie Dyn. Géographie Phys.* **1986**, *27*, 193–203.
79. Chalot-Prat, F. Pétrogénèse d'un Volcanisme Intracontinental Tardi-Orogénique Hercynien. Etude du Complexe Volcanique Carbonifère du Tazekka et de Zones Volcaniques Comparables dans le Mekam et la Région de Jerada (Maroc Oriental). Ph.D. Thesis, P. et M. Curie, Paris, France, 1990.
80. Chakib, A.; Aït Brahim, L.; Tahiri, A. Tectonique cassante et paléochamps de contraintes dans les régions de Bou Chahraine, d'el Jemaa Moud Bled et Merzaga du Permien à l'actuel (bordure méridionale du bassin de Rommani-Khémisset). In Proceedings of the 13 éme Colloque des Bassins Sédimentaires Marocains, Marrakech, Morocco, 19–22 March 1996; pp. 69–70.
81. Aït Brahim, L.; Tahiri, A.; Saidi, A. Proposition d'une nouvelle chronologie des événements tectoniques responsables de la structuration du bassin sur décrochement permien de Bou-Achouch (bordure septentrionale de la Meseta central). In Proceedings of the 13 éme Colloque des Bassins Sédimentaires Marocains, Marrakech, Morocco, 19–22 March 1996; pp. 9–10.
82. Hmich, D.; Schneider, J.W.; Saber, H.; Voigt, S.; El Wartiti, M. New continental Carboniferous and Permian faunas of Morocco: Implications for biostratigraphy, palaeobiogeography and palaeoclimate. *Geol. Soc. Spec. Publ.* **2006**, *265*, 297–324. [CrossRef]
83. Kerp, H.; Broutin, J.; Lausberg, S.; Aassoumi, H. Discovery of Latest Carboniferous–Early Permian radially symmetrical peltaspermaceous megasporophylls from Europe and North Africa. *C. R. Acad. Sci. Ser. IIA Earth Planet. Sci.* **2001**, *332*, 513–519. [CrossRef]
84. Jébrak, M. Contribution à l'histoire Naturelle des Filons (F, Ba) du Domaine Varisque Français et Marocain. Essai de Caractérisation Structurale et Géochimique des Filons en Extension et en Décrochement. Ph.D. Thesis, Univiversity of Orleans, Orleans, France, 1984.
85. Aassoumi, H.; Broutin, J.; Youbi, N. Découverte de Scleromedulloxylon cf. aveyronense, bois fossile de coniférophyte, dans le complexe volcanique permien du bassin de Khnifra (Maroc): Intérêt stratigraphique et floristique. *Ann. Paléontol.* **1995**, *81*, 1–16.
86. Youbi, N. Le complexe volcanique permien de Khenifra (SE du Maroc central): Cartographie, volcanologie, minéralogie, géochimie, considérations structurales et implications géodynamiques. Ph.D. Thesis, Cadi Ayyad University, Marrakesh, Morocco, 1990.
87. Youbi, N.; Gaggero, L.; Assafar, H.; Hadimi, I.; Boumehdi, M.A.; Bensalah, M.K.; Linnemann, U.; Gaertner, A.; Mata, J.; Doblas, M.; et al. U-Pb Zircon Geochronological and Petrologic Constraints on the PostCollisional Variscan Volcanism of the Khénifra Basin (Western Meseta, Morocco): Stratigraphic and Petrogenetic Implications. In Proceedings of the 2nd International Congress on Permian and Triassic, Casablanca, Morocco, 25–27 April 2018; pp. 53–54.
88. Van Houten, F. Late Variscan Nonmarine Basin Deposits, Northwest Africa: Record of Hercynotype Orogeny. In *The Continental Permain in Central, West, and South Europe*; Springer: Dordrecht, The Netherlands, 1976; pp. 215–224.
89. Hadimi, I.; Ait Lahna, A.; Assafar, H.; Tassinari, C.C.G.; Youbi, N.; Boumehdi, M.; Bensalah, M.K.; Gaggero, L.; Mata, J.; Doblas, M. The Post-Collisional Hercynian Volcanism of Rehamna, Western Meseta, Morocco. Mineral Chemistry, Petrology and U-Pb Dating. In Proceedings of the 2nd International Congress on Permian and Triassic, Casablanca, Morocco, 25–27 April 2018; pp. 33–35.
90. Baudin, T.; Chèvremont, P.; Razin, P.; Youbi, N.; Andries, D.; Hoepffner, C.; Tegyey, M. Carte géologique du Maroc au 1/50000, feuille de Skhour des Rehamna, Mémoire explicatif. *Notes Mém. Serv. Géol. Maroc* **2003**, *435*, 114.
91. Bensalah, M.K. De la fin du cycle orogénique hercynien à l'ouverture et l'évolution de l'Atlantique Central: Les marqueurs magmatiques de cette transition. Etude pétrologique et géochimique. Exemple d'application dans le Permien, le TriasJurassique et le Jurassique-Cré. Ph.D. Thesis, CAADi AYYAD, Marrakesh, Morocco, 2012.

92. Bensalah, M.K.; Youbi, N.; Ait Lahna, A.; Tassinari, C.C.G.; Boumehdi, M.A.; Basei, M.A.S.; Sato, K.; Aarab, E.M.; Mata, J. Geochemical and Geochronological Constraints on the Origin of the Intermediate and Felsic Dyke and Sill Swarms from the Western Meseta and the High Atlas (Morocco): Implications for Tectonic Evolution. In Proceedings of the 2nd International Congress on Permian and Triassic, Casablanca, Morocco, 25–27 April 2018; pp. 20–22.
93. Hoepffner, C. Le magmatisme pré- et post-orogénique hercynien dans le Paléozoïque des Rehamna. *Serv. Géologique du Maroc Rabat* **1982**, *303*, 150–163.
94. Charif, A. Etude Pétrographique et Géochimique du Volcanisme "Post-Collisionnel" du Permien Inférieur (Autunien) des Rahamna (Mechraâ Ben Abbou et Nazt Lararcha, Messta-Maroc): Implications Géochimiques, Pétrogénétiques et Géodynamiques. Ph.D. Thesis, University of Chouaib Doukkali, El Jadida, Morocco, 2001.
95. Razin, P.; Baudin, T.; Chèvremont, P.; Andries, D.; Youbi, N.; Hœpffner, C.; Thiéblemont, D.; Chihani, E. Carte géologique du Maroc au 1/50 000, feuille de Jebel Kharrou, Mémoire explicatif. *Notes Mém. Serv. Géol. Rabat* **2003**, *436*, 1–105.